Nuclear Spin-Lattice Relaxation in Magnetic Insulators*

D. BEEMAN† AND P. PINCUS‡
Department of Physics, University of California, Los Angeles, California

(Received 18 August 1967)

First-order nuclear spin-lattice relaxation arises in magnetic insulators when a nuclear spin directly interacts with one or more spin waves via the hyperfine interaction. The direct process, in which a single magnon is emitted, is not ordinarily allowed on the basis of energy conservation, since the energy of a nuclear spin flip is considerably lower than the minimum energy of a spin wave. When the hyperfine interaction is isotropic and the axes of quantization of the nuclear and electronic spins are collinear, the conservation of the z component of spin angular momentum forbids the Raman process, in which a thermal magnon is scattered to a state of different wave vector, accompanied by a nuclear spin flip. The three-magnon process is usually allowed. We consider here some second-order two- and three-magnon processes which arise when a virtual magnon, emitted in the direct process, is scattered by thermal magnons via the exchange interaction or the magnetic dipole-dipole interaction. This is possible, since (1) the magnon spectrum is lifetime broadened to overlap the nuclear spin resonance frequency, and (2) the dipole interaction does not conserve spin angular momentum. The second-order three-magnon process, arising from the four-magnon exchange interaction, enhances the three-magnon process relaxation rate by a factor of 8 in ferromagnets, and results in a temperature-dependent enhancement of about one order of magnitude in antiferromagnets. Three-magnon terms in the dipole-dipole interaction may induce a two-magnon process in both ferromagnets and antiferromagnets, which is of significance when the first-order Raman process is forbidden. We also calculate the relaxation rate due to a second-order exchange-scattering-induced two-magnon process which is often more important than the first-order process in canted antiferromagnets of both the "easy-axis" and the "hard-axis" anisotropy type.

I. INTRODUCTION

RECENT measurements of the nuclear spin-lattice relaxation time in extremely pure magnetic insulators[1–3] have resulted in renewed interest in intrinsic processes of nuclear spin-lattice relaxation. The first theoretical treatments of intrinsic nuclear spin-lattice relaxation processes in magnetic insulators were presented by Moriya[4] and by Van Kranendonk and Bloom[5] in 1956. Although they obtained qualitative agreement between theory and the experiments of Hardeman *et al.*,[6] it has only been recently that improved techniques of sample preparation have permitted experiments in which impurity-dominated relaxation processes have been excluded. These recently obtained experimental results[1,2] agree well with theory.

We consider here nuclear spin-lattice relaxation in pure, single domain, insulating ferromagnets and antiferromagnets at temperatures small compared with their Curie or Néel temperatures. Under these conditions, the principal relaxation mechanism will be the excitation of spin waves in the electron spin system via the hyperfine interaction. When the electron-nucleus magnetic dipole interaction is large enough to be significant, it may be included in the hyperfine interaction. Since the electron spins are tightly coupled to each other by exchange interactions, and interact with the crystal lattice much more strongly than with the nuclear spins, we may consider the electronic spin system to be always in thermal equilibrium with the crystal lattice. Hence, the word "lattice" will be used interchangeably with "electron spin system."

Section II reviews the theory of first-order spin-lattice relaxation processes, in which a nuclear spin relaxes by directly interacting with one or more spin waves via the hyperfine interaction. One-, two-, and three-magnon processes are discussed in both ferromagnets and antiferromagnets.

The following sections present the theory of some second-order processes involving spin-wave interactions, with virtual intermediate states, which may enhance or supersede the first-order processes. Relaxation rates are calculated for all processes considered. Section III discusses the previously proposed enhancement of the ferromagnetic three-magnon relaxation rate by exchange scattering,[7] and extends the theory to the antiferromagnetic case. In Sec. IV it is shown that the exchange interaction makes possible a second-order two-magnon relaxation process in canted antiferromagnets which can be competitive with the first-order two-magnon process. We consider both antiferromagnets possessing "easy-axis" anisotropy and "hard-axis" anisotropy. Section V discusses an analogous second-order two-magnon process which is induced by the electron magnetic dipole-dipole interaction. This mech-

* Supported in part by the National Science Foundation and the U.S. Office of Naval Research under Contract No. Nonr 233(88).

† Present address: Theoretical Division, Atomic Energy Research Establishment, Harwell, Didcot, Berkshire, England.

‡ Alfred P. Sloan Foundation Fellow.

[1] N. Kaplan, R. Loudon, V. Jaccarino, H. J. Guggenheim, D. Beeman, and P. A. Pincus, Phys. Rev. Letters **17**, 357 (1966).

[2] A. Narath and A. T. Fromhold, Jr., Phys. Rev. Letters **17**, 354 (1966).

[3] L. B. Welsh, Phys. Rev. **156**, 370 (1967).

[4] T. Moriya, Progr. Theoret. Phys. (Kyoto) **16**, 23 (1956); **16**, 641 (1956).

[5] J. Van Kranendonk and M. Bloom, Physica **22**, 545 (1956).

[6] G. E. G. Hardeman, N. J. Poulis, and W. van der Lugt, Physica **22**, 48 (1956).

[7] P. Pincus, Phys. Rev. Letters **16**, 398 (1966).

anism is operative in both ferromagnets and antiferromagnets.

II. FIRST-ORDER SPIN-LATTICE RELAXATION PROCESSES

A. Direct Relaxation Process

If the hyperfine interaction is isotropic, and the axes of quantization of the electronic and nuclear spins are collinear, we may write

$$A\mathbf{I}_j\cdot\mathbf{S}_j=\tfrac{1}{2}A(I_j^+S_j^-+I_j^-S_j^+ +2I_j^zS_j^z). \quad (2.1)$$

Here A is the strength of the isotropic hyperfine interaction, and the raising and lowering operators for the nuclear spin at the jth site are defined as $I_j^{\pm}=I_{jx}\pm iI_{jy}$. For ferromagnets, the transformation developed by Holstein and Primakoff[8] expresses the electronic spin raising and lowering operators as follows:

$$S_j^+=S_{jx}+iS_{jy}=(2S/N)^{1/2}\{\sum_{\mathbf{k}}\exp(-i\mathbf{k}\cdot\mathbf{r}_j)b_{\mathbf{k}}-(4SN)^{-1}\sum_{\mathbf{k},\mathbf{k}',\mathbf{k}''}\exp[i(\mathbf{k}-\mathbf{k}'-\mathbf{k}'')\cdot\mathbf{r}_j]b_{\mathbf{k}}^{\dagger}b_{\mathbf{k}'}b_{\mathbf{k}''}+\cdots\}, \quad (2.2a)$$

$$S_j^-=S_{jx}+iS_{jy}=(2S/N)^{1/2}\{\sum_{\mathbf{k}}\exp(i\mathbf{k}\cdot\mathbf{r}_j)b_{\mathbf{k}}^{\dagger}-(4SN)^{-1}\sum_{\mathbf{k},\mathbf{k}',\mathbf{k}''}\exp[i(\mathbf{k}+\mathbf{k}'-\mathbf{k}'')\cdot\mathbf{r}_j]b_{\mathbf{k}}^{\dagger}b_{\mathbf{k}'}^{\dagger}b_{\mathbf{k}''}+\cdots\}, \quad (2.2b)$$

$$S_{jz}=S-N^{-1}\sum_{\mathbf{k},\mathbf{k}'}\exp[i(\mathbf{k}-\mathbf{k}')\cdot\mathbf{r}_j]b_k^{\dagger}b_{k'}, \quad (2.2c)$$

where N is the number of spins in the solid. $\mathbf{r}_j$ denotes the position of the jth spin $\mathbf{S}_j$, and $b_{\mathbf{k}}^{\dagger}$ and $b_{\mathbf{k}}$ are the boson operators for the creation and annihilation of spin waves of wave vector $\mathbf{k}$. In the antiferromagnetic case, the spin system is divided into two interpenetrating sublattices denoted by the subscripts i and j, such that spins on sublattice i will have all nearest neighbors on sublattice j, and vice versa. For systems with easy-axis anisotropy, the effect of the crystalline anisotropy energy may be represented by a magnetic field H_A, which tends to align the spins $\mathbf{S}_i$ in the $+z$ direction and the spins $\mathbf{S}_j$ in the $-z$ direction. The spin-deviation operators for the two sublattices are defined in a manner analogous to the ferromagnetic case.[9] We define

$$\begin{aligned}
S_i^+&=(2S/N)^{1/2}\{\sum_{\mathbf{k}}\exp(-i\mathbf{k}\cdot\mathbf{r}_i)c_{\mathbf{k}}+\cdots\},\\
S_i^-&=(2S/N)^{1/2}\{\sum_{\mathbf{k}}\exp(i\mathbf{k}\cdot\mathbf{r}_i)c_{\mathbf{k}}^{\dagger}+\cdots\},\\
S_i^z&=S-N^{-1}\sum_{\mathbf{k},\mathbf{k}'}\exp[i(\mathbf{k}-\mathbf{k}')\cdot\mathbf{r}_i]c_{\mathbf{k}}^{\dagger}c_{\mathbf{k}'},\\
S_j^+&=(2S/N)^{1/2}\{\sum_{\mathbf{k}}\exp(-i\mathbf{k}\cdot\mathbf{r}_j)d_{\mathbf{k}}^{\dagger}+\cdots\},\\
S_j^-&=(2S/N)^{1/2}\{\sum_{\mathbf{k}}\exp(i\mathbf{k}\cdot\mathbf{r}_j)d_{\mathbf{k}}+\cdots\},\\
S_j^z&=-S+N^{-1}\sum_{\mathbf{k},\mathbf{k}'}\exp[-i(\mathbf{k}-\mathbf{k}')\cdot\mathbf{r}_j]d_{\mathbf{k}}^{\dagger}d_{\mathbf{k}'}, \quad (2.3)
\end{aligned}$$

where N is the number of spins on each sublattice and $c_{\mathbf{k}}^{\dagger}$ and $d_{\mathbf{k}}^{\dagger}$ are spin-wave creation operators for the i and j sublattices, respectively. In order to diagonalize the Hamiltonian it is necessary to make a transformation[9] to new spin-wave operators for the normal modes of oscillation,

$$\begin{aligned}
c_{\mathbf{k}}&=u_k\alpha_{\mathbf{k}}+v_k\beta_{\mathbf{k}}^{\dagger},\\
d_{\mathbf{k}}&=u_k\beta_{\mathbf{k}}+v_k\alpha_{\mathbf{k}}^{\dagger}, \quad (2.4)
\end{aligned}$$

with

$$2u_kv_k=(-\omega_e\gamma_K/\omega_k)$$

and

$$u_k^2+v_k^2=(\omega_e+\omega_A)/\omega_k, \quad (2.5)$$

where

$$\hbar\omega_e=g\beta H_e=2JzS \quad (2.6)$$

and

$$\hbar\omega_A=g\beta H_A. \quad (2.7)$$

For small k, and $\omega_e\gg\omega_A$, the frequency of an antiferromagnetic spin wave is given by

$$\omega_k\approx[2\omega_e\omega_A+\omega_e^2b^2k^2a^2]^{1/2} \quad (2.8)$$

for cubic lattices. The parameter b^2 is a fraction equal to $2/z$, where z is the number of nearest neighbors.

The first term of (2.1) provides us with a mechanism for nuclear spin-lattice relaxation. The I_j^+ operator relaxes the nuclear spin of the ith atom, while the S_j^- flips the electronic spin, creating a spin wave. The relaxation of the nuclear spins toward their equilibrium orientation is characterized by a nuclear spin-lattice relaxation time T_1.[10]

If W designates the probability of a transition from a state characterized by a nuclear spin quantum number m to one of $m+1$, then the spin-lattice relaxation time is given by the relation[11]

$$T_1=(I-m)(I+m+1)/2W. \quad (2.9)$$

The transition probability is given by Fermi's golden

[8] T. Holstein and H. Primakoff, Phys. Rev. **58**, 1098 (1940).
[9] See, e.g., F. Keffer, in *Handbuch der Physik*, edited by S. Flügge (Springer-Verlag, Berlin, 1966), Vol. 18, pt. 2.
[10] For a review of nuclear magnetic resonance and relaxation in antiferromagnets see V. Jaccarino, in *Magnetism*, edited by G. T. Rado and H. Suhl (Academic Press Inc., New York, 1965), Vol. 2A, Chap. 5.
[11] N. Bloembergen, E. M. Purcell, and R. V. Pound, Phys. Rev. **73**, 679 (1948).

rule to be

$$W=(2\pi/\hbar)\sum_f |\langle f|\mathcal{H}'|i\rangle|^2\delta(E_i-E_f), \quad (2.10)$$

where $\mathcal{H}'$ designates the interaction inducing the transition, i and f designate the initial and final states of the electronic-nuclear spin system, and the δ function insures the conservation of energy in the transition.

The simplest interaction capable of producing nuclear spin-lattice relaxation is that obtained by expanding S_j^- to first order in spin-wave operators and substituting it into the first term of (2.1). For a ferromagnet, with $\mathbf{r}_j\equiv 0$,

$$\mathcal{H}'=\tfrac{1}{2}AI^+(2S/N)^{1/2}\sum_{\mathbf{k}} b_{\mathbf{k}}^\dagger. \quad (2.11)$$

This is represented diagrammatically in Fig. 1. Since the relaxing nuclear spin flips an electronic spin down, creating a spin wave, the z component of spin angular momentum is conserved. The energy-conservation requirement of (2.10) is more difficult to ensure, however. The δ function demands that AS, the change in energy due to the nuclear spin flip, be equal to the energy of the spin wave created. This is usually not possible, since applied dc magnetic fields of the magnitude needed to ensure single domain behavior of the sample will cause $g\beta H$, the minimum energy of a ferromagnetic spin wave, to be much greater than AS.

FIG. 1. The "direct process" of nuclear spin-lattice relaxation in a ferromagnet. The "X" denotes a nuclear spin flip.

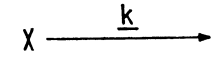

Furthermore, the crystalline anisotropy fields encountered are generally large enough to make $g\beta H>AS$, even with no external field present. It is even more difficult to satisfy energy conservation with this process in the antiferromagnetic case. Here the energy gap in the spin-wave spectrum is $g\beta(2H_AH_e)^{1/2}$, which is usually even larger than the ferromagnetic energy gap, because of the large magnitude of H_e, the exchange field. Thus the direct process, involving a single spin wave, is rarely of significance.

B. Raman Relaxation Process

The two-magnon, or Raman, process illustrated in Fig. 2 does not present this difficulty. Here we have a spin wave of wave vector $\mathbf{k}$ being annihilated and another of wave vector $\mathbf{k}'$ being created, as the nuclear spin flips. The energy-conservation requirement demands that $AS+E_k=E_{k'}$. This is easily satisfied. However, a problem arises with the conservation of the longitudinal component of spin angular momentum, since there is a nuclear spin flip, with no net change in electron spin. In fact, an examination of (2.1) reveals that there is no term which can be put in the form $I^+b_{\mathbf{k}'}{}^\dagger b_{\mathbf{k}}$. However, there are circumstances under which the Raman process may occur. If the hyperfine interaction is anisotropic, the conservation of the z component of angular momentum is not required, as evidenced by the nonvanishing commutator, $[S_z+I_z, \mathcal{H}]$. There will then be terms of the form $A_{xz}I_xS_z$, which will induce a Raman process. Also, if the hyperfine interaction is isotropic but there is an angle θ between the axes of quantization of the nuclear and electronic spins, there will be a term equal to $\frac{1}{2}AI^+S_z\sin\theta$ causing nuclear spin-lattice relaxation by a two-magnon process. If the material has a preferred direction of electron-spin alignment, such an angle may arise from an external field H normal to the electron-spin axis. The nuclear-spin axis will then be tilted by an angle $\theta=\tan^{-1}H/H_{\rm hf}$, where the hyperfine field at the nucleus is $H_{\rm hf}=AS/g_N\mu_N$. In the case of antiferromagnets, the field H will also cant the ordinarily antiparallel electron spin sublattices towards each other, deviating from the preferred axis by an angle $\phi=\tan^{-1}[H/(2H_e+H_A)]$. If this canting is small, it will have little effect on the spin-wave spectrum and may be ignored. This effect will be considered in more detail in Sec. IV.

FIG. 2. The Raman process of nuclear spin-lattice relaxation in a ferromagnet.

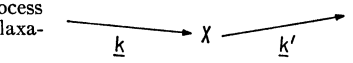

Nuclear spin-lattice relaxation rates for the two-magnon process were first calculated for antiferromagnets by Moriya[4] and by Van Kranendonk and Bloom.[5] The calculation for a ferromagnet was made by Mitchell.[12] For the sake of completeness, we will sketch out these calculations.

The ferromagnetic Raman-process calculation will be presented here in some detail, since it involves many of the assumptions and approximations made in the calculations in the following sections.

If the axis of nuclear-spin quantization is tilted from the axis of quantization of the ferromagnetic spins by an angle θ, the interaction producing nuclear spin-lattice relaxation is

$$\mathcal{H}'=-(A/2N)I^+\sin\theta\sum_{\mathbf{k},\mathbf{k}'} b_{\mathbf{k}}^\dagger b_{\mathbf{k}'}. \quad (2.12)$$

Using $\mathcal{H}'$ in (2.10), we obtain from (2.9)

$$(1/T_1)=(4\pi/\hbar)(A/2N)^2\sin^2\theta \times\sum_{\mathbf{k},\mathbf{k}'} n_{k'}(1+n_k)\delta(E_k-E_{k'}-AS), \quad (2.13)$$

where n_k is the Bose-Einstein distribution function

$$\langle b_{\mathbf{k}}^\dagger b_{\mathbf{k}}\rangle=n_k=[\exp E_k/k_BT-1]^{-1}, \quad (2.14)$$

where T is the lattice temperature and k_B is the Boltzmann constant. The energy of the nuclear spin

FIG. 3. The three-magnon process of nuclear spin-lattice relaxation in a ferromagnet.

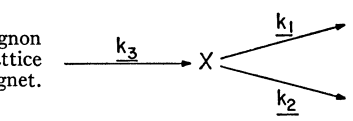

[12] A. Mitchel, J. Chem. Phys. **27**, 17 (1957).

flip, AS, may be neglected in comparison with the spin-wave energy E_k. Replacing the sums by integrals, we obtain

$$T_1^{-1}=\frac{4\pi}{\hbar}\left(\frac{A}{2N}\right)^2\sin^2\theta\,\frac{V^2}{(2\pi)^6}\,(4\pi)^2\int_0^{k_{\max}}\int_0^{k_{\max}}k^2dk\,k'^2dk'$$
$$\times\frac{\exp(E_k/k_BT)}{[\exp(E_k/k_BT)-1]^2}\,\delta(E_k-E_{k'}),\qquad(2.15)$$

where V, the volume of the sample, is equal to Na^3 for a simple cubic lattice. For small k,

$$E_k\approx g\beta H+2JSk^2a^2.\qquad(2.16)$$

We note that for $k_BT\ll 2JS$, n_k will be very small for large k. Therefore we may use the small k approximation for E_k, and replace the upper limit of the integrals by infinity for $k_BT\ll 2JS$. Expressing k in terms of E_k, we obtain

$$T_1^{-1}=\frac{A^2}{\hbar}\,\frac{\sin^2\theta}{2(2\pi)^3(\hbar\omega_e)^3}$$
$$\times\int_{g\beta H}^{\infty}dE(E-g\beta H)\,\frac{\exp(E/k_BT)}{[\exp(E/k_BT)-1]^2},\qquad(2.17)$$

where $\hbar\omega_e=2JS$. By defining $x=E/k_BT$ and $x_0=g\beta H/k_BT$, we obtain

$$T_1^{-1}=\frac{A^2}{\hbar^2\omega_e}\,\frac{\sin^2\theta}{2(2\pi)^3}\left(\frac{k_BT}{\hbar\omega_e}\right)^2\int_{x_0}^{\infty}\frac{dx}{e^x-1}.\qquad(2.18)$$

In the limit $g\beta H\ll k_BT$, this becomes

$$T_1^{-1}=\frac{A^2}{\hbar^2\omega_e}\,\frac{\sin^2\theta}{2(2\pi)^3}\left(\frac{k_BT}{\hbar\omega_e}\right)^2\ln\left(\frac{k_BT}{g\beta H}\right).\qquad(2.19)$$

The calculation for the antiferromagnetic case proceeds in an analogous manner, with the result

$$T_1^{-1}=\frac{A^2}{\hbar^2\omega_e}\,\frac{8\sin^2\theta}{(2\pi)^3b^6}\left(\frac{k_BT}{\hbar\omega_e}\right)^3\int_{T_{AE}/T}^{\infty}\frac{x\,dx}{e^x-1},\qquad(2.20)$$

where T_{AE} is defined by $k_BT_{AE}=\hbar\omega_{AE}=g\beta(2H_eH_A)^{1/2}$. Note that $\hbar\omega_e=2JzS$ in the antiferromagnetic case. For $T\gg T_{AE}$, the integral approaches a maximum value of $\frac{1}{6}\pi^2$. For $T\ll T_{AE}$, the integral is approximately equal to $(T_{AE}/T)\exp(-T_{AE}/T)$. For intermediate temperatures, the integral may be expressed in terms of the commonly tabulated Debye integral.[13] Equation (2.20) was used by Moriya to explain the results of measurements of the nuclear spin-lattice relaxation time of protons in antiferromagnetic $CuCl_2\cdot 2H_2O$ by Hardeman.[6] When θ was varied by means of a magnetic field applied perpendicular to the axis of quantization of the electronic spins, the spin-lattice relaxation rate was found to vary according to $\sin^2\theta$, as predicted. However, the measured values of T_1 had a much stronger temperature dependence than that predicted by the theory. This disagreement is understandable in view of the fact that the small k approximation was made even though the condition $k_BT\ll\hbar\omega_e$ was not very well satisfied. Furthermore, there is no guarantee that the samples were pure enough to exclude the effect of impurity-dominated relaxation processes. Because of the difficulty in obtaining samples of sufficient purity to permit observation of intrinsic spin-lattice relaxation processes, good quantitative agreement of theory and experiment was not obtained until 10 years later with the experiments of Kaplan *et al.*[1] In these experiments, the spin-lattice relaxation time of the F^{19} nucleus in extremely pure crystals of MnF_2 was measured. The angle of θ was varied by means of an applied magnetic field. The results are in excellent agreement with the Raman-process theory over a variation of $1/T_1$ of six orders of magnitude, as the temperature was varied from 3.2 to 26°K. The application of this theory to the particular case of MnF_2 is discussed in more detail in Ref. 1.

C. Three-Magnon Relaxation Process

If the hyperfine interaction is isotropic and the electronic and nuclear axes of quantization are collinear, we must go to a three-magnon process to find a means of relaxation compatible with energy and momentum conservation requirements. By expanding $\frac{1}{2}AI^+S^-$ to third order in magnon operators, we obtain

$$\mathcal{H}'=(-A/8SN)(2S/N)^{1/2}\sum_{\mathbf{k}_1,\mathbf{k}_2,\mathbf{k}_3}b_{\mathbf{k}_1}{}^{\dagger}b_{\mathbf{k}_2}{}^{\dagger}b_{\mathbf{k}_3},\qquad(2.21)$$

which gives rise to the process shown in Fig. 3. The net effect of the two creation operators and one annihilation operator is to flip a single electron spin when the nuclear spin relaxes, thus conserving angular momentum. Energy is conserved by the requirement that the spin-wave energies obey the relation $E_1+E_2=E_3$. The use of (2.21) in the relaxation rate (2.20) gives the result obtained by Oguchi and Keffer,[14]

$$T_1^{-1}=(A^2/\hbar^2\omega_e)[7.6/16S(2\pi)^5](k_BT/\hbar\omega_e)^{7/2}\qquad(2.22)$$

for $k_BT\gg g\beta H$. The factor of 7.6 is obtained from an integral which reaches its maximum value when the parameter $g\beta H/k_BT$ is much less than unity. This limit is a realistic one for experiments involving ferromagnets, since $g\beta H$ is generally on the order of tenths of a degree Kelvin. For antiferromagnets, the energy gap in the spin-wave spectrum is usually much larger and may not be ignored.

In the antiferromagnetic case, we expand S_i^- to third order in spin-wave operators, apply the transformation (2.4), and obtain

$$\mathcal{H}'=(-A/8SN)(2S/N)^{1/2}I^+\sum_{\mathbf{k}_1,\mathbf{k}_2,\mathbf{k}_3}\{u_1u_2u_3\alpha_1{}^{\dagger}\alpha_2{}^{\dagger}\alpha_3$$
$$+2u_1v_2u_3\alpha_1\beta_2\alpha_3{}^{\dagger}+2v_1u_2v_3\beta_1{}^{\dagger}\alpha_2{}^{\dagger}\beta_3+v_1v_2v_3\beta_1\beta_2\beta_3{}^{\dagger}\},\qquad(2.23)$$

[13] See, e.g., *Handbook of Mathematical Functions*, edited by M. Abramowitz and I. A. Stegen (U.S. Government Printing Office, Washington, D.C., 1964), p. 998.

[14] T. Oguchi and F. Keffer, J. Phys. Chem. Solids **25**, 405 (1964).

where the subscripts on the transformation coefficients and the creation and annihilation operators refer to the wave vectors $\mathbf{k}_1$, $\mathbf{k}_2$, and $\mathbf{k}_3$. The use of the above expression in the golden rule relaxation-rate equation gives

$$T_1^{-1}=(2\pi/\hbar)(A^2/16N^3S)\sum_{\mathbf{k}_1,\mathbf{k}_2,\mathbf{k}_3}\{(u_1u_2u_3)^2+4(u_1v_2u_3)^2+4(u_1v_2v_3)^2+(v_1v_2v_3)^2\}n_1n_2(1+n_3)\delta(E_1+E_2-E_3). \quad (2.24)$$

Using the long-wavelength approximation of the spin-wave dispersion relation (2.8) and making the approximation $u_k^2\approx v_k^2\approx\omega_e/2\omega_k$, we obtain

$$T_1^{-1}=(A^2/\hbar^2\omega_e)[5/S(2\pi)^5b^9](k_BT/\hbar\omega_e)^5I_3(T_{AE}/T). \quad (2.25)$$

The temperature-dependent integral $I_3(T_{AE}/T)$ is given by

$$I_3(T_{AE}/T)=\int_{x_{AE}}^{\infty}\int_{x_{AE}}^{\infty}\frac{(x_1^2-x_{AE}^2)^{1/2}(x_2^2-x_{AE}^2)^{1/2}[(x_1+x_2)^2-x_{AE}^2]^{1/2}e^{x_1+x_2}}{(e^{x_1}-1)(e^{x_2}-1)(e^{x_3}-1)}dx_1dx_2, \quad (2.26)$$

where $x_{AE}=T_{AE}/T=\hbar\omega_{AE}/k_BT$. For high temperatures, the integral approaches its maximum value of 8.6. Since the temperature dependence of the integral generally cannot be ignored, $I_3(T_{AE}/T)$ is plotted as a function of T/T_{AE} in Fig. 4. At this point, it is worthwhile to test the validity of the small k approximation by means of a comparison with an exact calculation based on the true magnon density of states. The magnon density of states function for MnF_2 derived by Allen, Loudon, and Richards[15] from neutron spectroscopic measurements[16] has a peak near the Brillouin zone boundary which can give a large contribution to the relaxation, despite the small occupation probability of these states. Proceeding from (2.24), Kaplan *et al.*[1] have calculated the three-magnon process contribution to $1/T_1$ for F^{19} in MnF_2 from this density-of-states function. The results of this calculation and those of the long-wavelength approximation calculation are plotted as a function of temperature in Fig. 5. A comparison of the two curves reveals that zone boundary effects become important in MnF_2 above 10°K.

Figure 5 does not give the entire three-magnon-process contribution to $1/T_1$, however. In the following section it will be shown that a second-order three-magnon process arising from the four-magnon terms in the exchange interaction can lead to an enhancement of the three-magnon process relaxation rate by an order of magnitude in both the ferromagnetic and the antiferromagnetic case.

The probability of the excitation of a thermal magnon is given by the Bose distribution function (2.14), which is very small when the magnon density of states is large. Therefore, processes involving large numbers of magnons will give smaller contributions to the relaxation rate than allowed processes with fewer magnons. Since the three-magnon process is usually allowed, it is not necessary to expand $\frac{1}{2}AI^+S^-$ to higher order in spin-wave operators.

[15] S. J. Allen, R. Loudon, and P. L. Richards, Phys. Rev. Letters **16**, 463 (1966).
[16] A. Okazaki, K. C. Turberfield, and R. W. H. Stevenson, Phys. Letters **8**, 9 (1964).

III. EXCHANGE-SCATTERING-ENHANCED THREE-MAGNON PROCESS

A. Ferromagnetic Case

If the ferromagnetic exchange interaction is expanded to fourth order in magnon operators, one obtains the exchange-scattering term, which is given in the long-wavelength limit by [9]

$$\mathcal{H}_{ex}=-(Ja^2/2N)\sum_{\mathbf{k}_1,\mathbf{k}_2,\mathbf{k}_3,\mathbf{k}_4}b_1^\dagger b_2^\dagger b_3b_4\times(\mathbf{k}_1\cdot\mathbf{k}_2+\mathbf{k}_3\cdot\mathbf{k}_4)\delta(\mathbf{k}_1+\mathbf{k}_2-\mathbf{k}_3-\mathbf{k}_4). \quad (3.1)$$

It has been shown[7] that a virtual magnon from the direct relaxation process may be scattered by a thermal magnon via this interaction. The result is a three-magnon process which enhances the three-magnon relaxation rate calculated in the previous section. This second-order process, illustrated in Fig. 6, takes place as follows:

(1) A nuclear spin flips and creates a virtual spin wave of wave vector $\mathbf{k}_4$ via the transverse part of the hyperfine interaction

$$\tfrac{1}{2}AI^+S^-=\tfrac{1}{2}A(2S/N)^{1/2}I^+\sum_{\mathbf{k}}b_{\mathbf{k}}^\dagger. \quad (3.2)$$

(2) The virtual magnon and a thermal magnon of wave vector $\mathbf{k}_3$ interact via (3.1) and are scattered to new spin-wave states of wave vector $\mathbf{k}_1$ and $\mathbf{k}_2$. The effective interaction is one in which the thermal magnon is destroyed and two magnons are created, accompanied by a nuclear spin flip. Second-order time-dependent perturbation theory gives the matrix element for this three-magnon process:

$$\mathcal{H}_{eff}=AI^+(2S/N)^{1/2}(Ja^2/2N)[b_1^\dagger b_2^\dagger b_3/E(\mathbf{k}_1+\mathbf{k}_2-\mathbf{k}_3)]\times[\mathbf{k}_1\cdot\mathbf{k}_2+\mathbf{k}_3\cdot(\mathbf{k}_1+\mathbf{k}_2-\mathbf{k}_3)]. \quad (3.3)$$

This equation includes the process in which $\mathbf{k}_3$ and $\mathbf{k}_4$ are interchanged.

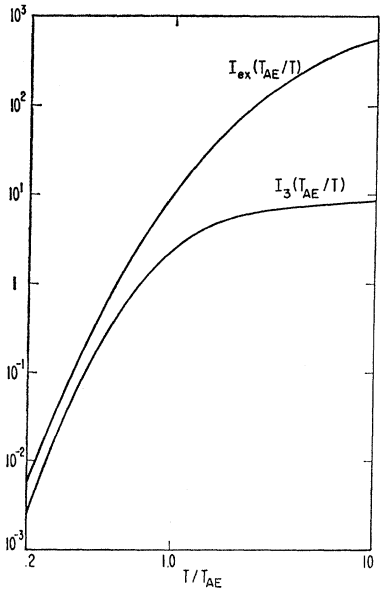

FIG. 4. The temperature-dependent integrals $I_3(T_{AE}/T)$ and $I_{ex}(T_{AE}/T)$, which occur in the calculation of the first-order antiferromagnetic three-magnon process relaxation rate, and the exchange-scattering-enhanced three-magnon process, respectively.

If $g\beta H \ll k_B T$, $E(\mathbf{k}_1+\mathbf{k}_2-\mathbf{k}_3) \approx 2JSa^2(\mathbf{k}_1+\mathbf{k}_2-\mathbf{k}_3)^2$ in the long-wavelength limit, giving an interaction independent of J. The total three-magnon process interaction, including $\mathcal{H}_{\text{eff}}$ plus the first-order interaction, (2.21) is then

$$\mathcal{H} = (-A/8SN)(2S/N)^{1/2} I^+ \times \sum_{\mathbf{k}_1,\mathbf{k}_2,\mathbf{k}_3} \left\{ 1 - \frac{2[\mathbf{k}_1\cdot\mathbf{k}_2 + \mathbf{k}_3\cdot(\mathbf{k}_1+\mathbf{k}_2-\mathbf{k}_3)]}{(\mathbf{k}_1+\mathbf{k}_2-\mathbf{k}_3)\cdot(\mathbf{k}_1+\mathbf{k}_2-\mathbf{k}_3)} \right\} b_1^\dagger b_2^\dagger b_3. \tag{3.4}$$

If we designate the quantity in the curly brackets by

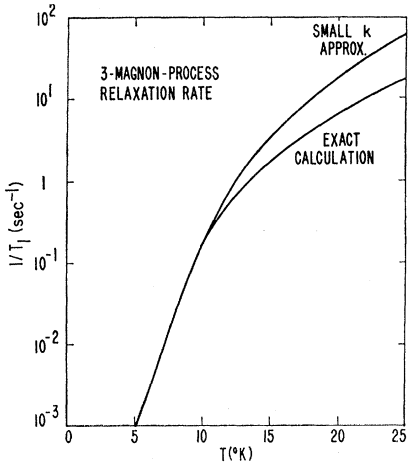

FIG. 5. The first-order three-magnon process relaxation rate of F^{19} in MnF_2 calculated with the exact spin-wave density of states, and with the small k approximation.

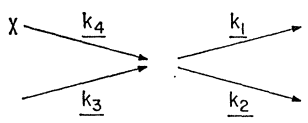

FIG. 6. The second-order ferromagnetic three-magnon nuclear spin-lattice relaxation process. The vertex corresponds to a scattering of spin waves via the exchange interaction.

$\{M\}$, we see that (3.4) differs from (2.21) by a factor of $\{M\}$; hence the enhancement in relaxation rate will be given by the angular average of $\{M\}^2$. Making use of the energy-conservation requirement $k_1^2+k_2^2=k_3^2$, and performing the angular integrations, we see that the angular average of $\{M\}^2$ is nearly independent of the magnitudes of k_1 and k_2, and is approximately equal to 8. Thus, the effect of exchange scattering is to multiply the relaxation rate given by (2.22) by a factor of 8. Narath and Fromhold[2] have calculated exchange-scattering-enhanced three-magnon spin-lattice relaxation rates for Cr^{53} in ferromagnetic $CrCl_3$, and have obtained good agreement between theory and their relaxation-time measurements.

B. Antiferromagnetic Case

A similar enhancement occurs for antiferromagnets as well. In the antiferromagnetic case, a virtual magnon may be created or absorbed via the hyperfine interaction

$$\tfrac{1}{2}AI^+S^- = \tfrac{1}{2}AI^+(2S/N)^{1/2}\sum_k u_k(\alpha_k^\dagger - \beta_k). \tag{3.5}$$

The virtual magnon interacts with thermal magnons via the antiferromagnetic exchange-scattering term,

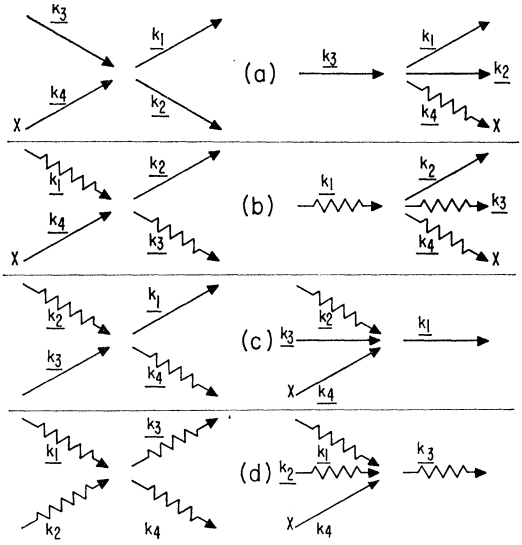

FIG. 7. The second-order three-magnon relaxation process in an antiferromagnet. The "X" denotes a nuclear spin flip accompanied by the emission or absorption of a virtual magnon. The straight and wiggly lines represent spin waves from the α and β branches of the spin wave spectrum, respectively. Each of the four processes a, b, c, and d may arise in two ways.

given in the long-wavelength limit by

$$\mathcal{H}_{ex}=(Jzb^2a^2/4N)$$
$$\times\sum_{k_1,k_2,k_3,k_4}[u_1u_2u_3u_4\alpha_1^\dagger\alpha_2^\dagger\alpha_3\alpha_4+4\alpha_1^\dagger\beta_2\alpha_3\beta_4^\dagger$$
$$-4\alpha_1\alpha_2\beta_3\alpha_4^\dagger-4\beta_1\beta_2\alpha_3\beta_4^\dagger+\beta_1^\dagger\beta_2^\dagger\beta_3\beta_4+\text{c.c.}]$$
$$\times(\mathbf{k}_1\cdot\mathbf{k}_2+\mathbf{k}_3\cdot\mathbf{k}_4)\delta(\mathbf{k}_1+\mathbf{k}_2-\mathbf{k}_3-\mathbf{k}_4). \quad (3.6)$$

Here $u_k\approx-v_k\approx(\omega_e/2\omega_k)^{1/2}$ and c.c. designates the complex conjugate of the terms enclosed in brackets. Figure 7 shows the eight possible diagrams which can result in four distinct second-order three-magnon relaxation processes. The effective Hamiltonian for these processes is

$$\mathcal{H}_{eff}=(A/2Sn)(2S/N)^{1/2}I^+$$
$$\times\sum_{k_1,k_2,k_3,k_4}u_1u_2u_3u_4^2(\hbar\omega_eb^2a^2/E_4)(\mathbf{k}_1\cdot\mathbf{k}_2+\mathbf{k}_3\cdot\mathbf{k}_4)$$
$$\times[\alpha_1^\dagger\alpha_2^\dagger\alpha_3-2\alpha_1^\dagger\beta_2\alpha_3+2\beta_1\alpha_2^\dagger\beta_3^\dagger-\beta_1\beta_2\beta_3^\dagger]$$
$$\times\delta(\mathbf{k}_1+\mathbf{k}_2-\mathbf{k}_3-\mathbf{k}_4). \quad (3.7)$$

Combining this with (2.23), the interaction producing first-order three-magnon relaxation, we obtain

$$\mathcal{H}'=-(A/8SN)(2SN)^{1/2}I^+$$
$$\times\sum_{k_1,k_2,k_3}u_1u_2u_3\{2M_1(\beta_1^\dagger\alpha_2^\dagger\beta_3-\alpha_1\beta_2\alpha_3^\dagger)$$
$$+M_2(\alpha_1^\dagger\alpha_2^\dagger\alpha_3-\beta_1\beta_2\beta_3^\dagger)\}, \quad (3.8)$$

where

$$M_1=\frac{k_{AE}^2+3k_1^2+k_2^2+k_3^2-4\mathbf{k}_1\cdot(\mathbf{k}_2+\mathbf{k}_3)}{k_{AE}^2+k_1^2+k_2^2+k_3^2-2k_1\cdot(\mathbf{k}_2+\mathbf{k}_3)+2\mathbf{k}_2\cdot\mathbf{k}_3} \quad (3.9)$$

and

$$M_2=\frac{k_{AE}^2+k_1^2+k_2^2+3k_3^2-4\mathbf{k}_3\cdot(\mathbf{k}_1+\mathbf{k}_2)}{k_{AE}^2+k_1^2+k_2^2+k_3^2-2k_3\cdot(\mathbf{k}_1+\mathbf{k}_2)+2\mathbf{k}_1\cdot\mathbf{k}_2}. \quad (3.10)$$

k_{AE} is defined by the relation $g\beta(2H_eH_A)^{1/2}=\hbar\omega_{AE}=\hbar\omega_ebak_{AE}$. Thus $\omega_k^2=\omega_e^2b^2a^2(k_{AE}^2+k^2)$. From (3.8), we obtain the spin-lattice relaxation rate

$$1/T_1=(2\pi/\hbar)(A/16N^3S)$$
$$\times\sum_{k_1,k_2,k_3}(u_1u_2u_3)^2(8M_1^2+2M_2^2)n_1n_2(1+n_3)$$
$$\times\delta(E_1+E_2-E_3). \quad (3.11)$$

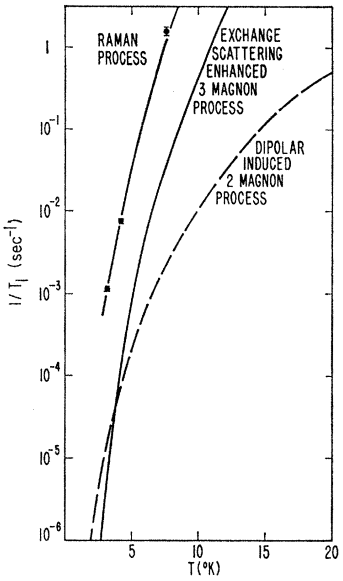

FIG. 8. The relaxation rate of F^{19} in MnF_2 calculated for the zero-field Raman process, the exchange-scattering-enhanced three-magnon process, and the dipolar induced two-magnon process. The experimental points are taken from Ref. 1.

This differs from the expression (2.24) for the three-magnon process relaxation rate without exchange-scattering enhancement by the angular dependent factors M_1^2 and M_2^2. Changing the sums to integrals and performing the angular integrations for (3.11) we obtain the angular averages $\langle M_1^2\rangle$ and $\langle M_2^2\rangle$. In the limit of $T\ll T_{AE}$ we find $\langle M_1^2\rangle\approx1.0$ and $\langle M_2^2\rangle\approx6.25$, giving an enhancement of $\frac{1}{10}(8M_1^2+2M_2^2)=2.05$. For $T\gg T_{AE}$,

$$\langle M_1^2\rangle\approx\tfrac{22}{3}+(k_2/k_1)\{\tfrac{1}{4}\pi[(k_1+k_2)/k_{AE}]-2\} \quad (3.12)$$

and

$$\langle M_2^2\rangle\approx\tfrac{16}{3}+\tfrac{1}{4}\pi[k_1k_2/k_{AE}(k_1+k_2)]. \quad (3.13)$$

Integrating over the magnitude of the wave vectors and assuming $k_BT\ll\hbar\omega_e$, we obtain a result similar to (2.25):

$$T_1^{-1}=(A^2/\hbar^2\omega_e)[5/S(2\pi)^5b^9](k_BT/\hbar\omega_e)^5I_{ex}(T_{AE}/T). \quad (3.14)$$

Here, the temperature-dependent integral $I_{ex}(T_{AE}/T)$ is given by

$$I_{ex}(T_{AE}/T)=\int_{x_{AE}}^\infty\int_{x_{AE}}^\infty\frac{(x_1^2-x_{AE}^2)^{1/2}(x_2^2-x_{AE}^2)^{1/2}[(x_1+x_2)^2-x_{AE}^2]^{1/2}e^{x_1+x_2}}{(e^{x_1}-1)(e^{x_2}-1)(e^{x_3}-1)}\tfrac{1}{10}(\langle8M_1^2\rangle+\langle2M_2^2\rangle)dx_1dx_2, \quad (3.15)$$

differing from (2.26) by the factors $\langle M_1^2\rangle$ and $\langle M_2^2\rangle$. As before, $x_{AE}=T_{AE}/T$. For $T\ll T_{AE}$,

$$I_{ex}(T_{AE}/T)\approx\tfrac{1}{2}[(2.05)\pi(3)^{1/2}](T_{AE}/T)^2\exp(-2T_{AE}/T). \quad (3.16)$$

In the limit $T\gg T_{AE}$,

$$I_{ex}(T_{AE}/T)\approx5\pi(T/T_{AE})\ln T/T_{AE}. \quad (3.17)$$

This last expression shows that the enhancement diverges for vanishing energy gap. It is not very useful

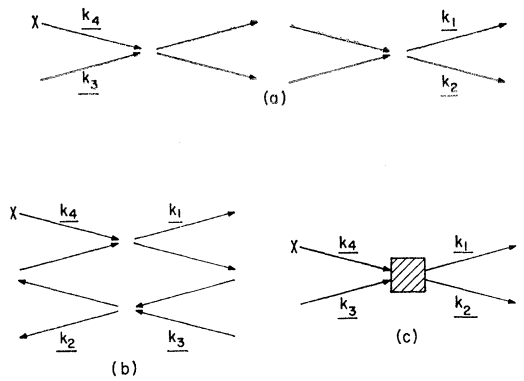

FIG. 9. (a) and (b) represent two possible higher-order three-magnon processes involving repeated exchange scatterings. (c) represents the effect of all such processes, summed to all orders.

for computational purposes, however, since it is valid only for temperatures quite a bit larger than T_{AE}. For typical values of T_{AE} and $\hbar\omega_e$, the long-wavelength approximation breaks down in this region. The results of a numerical integration of (3.5) are shown in Fig. 4, where $I_{ex}(T_{AE}/T)$ is plotted as a function of T/T_{AE}. The temperature-dependent integral $I_3(T_{AE}/T)$ for the antiferromagnetic three-magnon process without exchange-scattering enhancement is also plotted in Fig. 4. From this one may see that the minimum enhancement is 2.05 for $T \ll T_{AE}$, and that the enhancement increases without limit for increasing temperature.

We should expect the enhanced three-magnon process to provide the dominant contribution to $1/T_1$ in a typical antiferromagnet having an isotropic hyperfine interaction and having collinear axes of quantization of the electronic and nuclear spins, although the dipolar-induced Raman process discussed in Sec. II may also give a significant contribution. There is another process which is of greater significance in the case of F^{19} nuclear spin-lattice relaxation in MnF_2, however. Each fluorine atom has three nearest-neighbor manganese atoms arranged in such a manner that the net effect, in the static limit, is a coupling of the F^{19} nuclear spin to a single Mn^{++} spin via an isotropic hyperfine interaction.[17,18] Thus there should be no contribution to the relaxation from the first-order Raman process discussed in the previous section. When finite wavelength spin waves are excited, however, the anisotropic contributions to the hyperfine interaction from different manganese spins do not cancel, and a significant first-order Raman process occurs. This process is discussed in more detail in Ref. 1. Figure 8 displays the calculated F^{19} relaxation rates in MnF_2 as a function of temperature for the three processes mentioned above. The relaxation rates measured by Kaplan *et al.*[1] are shown as well, and conform quite closely to the theoretical curve for this first-order Raman process.

It has been pointed out by Holstein[19] that repeated exchange scatterings may further enhance the relaxation rate. Figures 9(a) and (b) diagrammatically represent some typical higher-order relaxation processes. The net effect of all repeated exchange scattering may be represented by Fig. 9(c), where the box includes all intermediate scatterings. Dyson[20] and others have calculated the exact exchange-scattering amplitude for the scattering of two magnons in an ideal Heisenberg ferromagnet. Such calculations are not applicable here, since they are based upon the assumption of energy conservation between the two incoming and the two outgoing spin waves. The relaxation mechanism which we consider here depends upon the fact that the energy spectrum of the magnon emitted in the direct relaxation process is lifetime broadened to include the energy of a nuclear spin flip. Thus, although there is the over-all conservation of energy in the effective three-magnon relaxation process, we may not demand the conservation of energy in the scattering process, as is done in the usual treatments of two-magnon scattering. The matrix element for the process shown in Fig. 9(c) could presumably be obtained by summing the diagrams of the form 9(a) and (b) to all orders. Since the matrix element for each individual exchange scattering is proportional to $(2S)^{-1}$, the summation should converge rapidly for $S \gg 1$, but may present more difficulty for $S=\frac{1}{2}$. Also, repeated exchange scattering could drastically affect the nuclear spin-lattice relaxation in antiferromagnets when the spin-wave energy gap is much less than k_BT. Since many antiferromagnets have an electronic spin greater than unity, and a comparatively high spin-wave energy gap, we may often neglect the effect of repeated scatterings. The calculation given here for MnF_2, for example, is probably reasonably accurate, since $S=\frac{5}{2}$ and $T_{AE}=12.5°K$. Nevertheless, a thorough investigation of the effects of repeated exchange scatterings would be of considerable interest.

IV. NUCLEAR SPIN-LATTICE RELAXATION IN CANTED ANTIFERROMAGNETS

A. Preliminaries

Many antiferromagnetic compounds have internal anisotropy fields which tend to cant the ordinarily antiparallel sublattices away from the preferred axis of alignment by an angle ϕ, resulting in a net transverse component of magnetization.[21] In a typical NMR experiment on such a material, a static magnetic field H is applied normal to the preferred axis, to increase the canting angle. Such a configuration is often used

[17] See, e.g., A. J. Freeman and R. E. Watson, in *Magnetism*, edited by G. T. Rado and H. Suhl (Academic Press Inc., New York, 1965), Vol. 2A.

[18] V. Jaccarino and R. G. Shulman, Phys. Rev. **107**, 1196 (1957).

[19] T. Holstein (private communication).

[20] F. J. Dyson, Phys. Rev. **102**, 1217 (1956).

[21] See, e.g., T. Moriya, in *Magnetism*, edited by G. T. Rado and H. Suhl (Academic Press Inc., New York, 1963), Vol. 1.

for antiferromagnets which ordinarily are not canted. An example of this is the measurement of the first-order Raman process nuclear spin-lattice relaxation of F^{19} in MnF_2, discussed in Sec. II. Usually, the internal canting field may be neglected in comparison with H, or included in H. Then the canting angle is approximately given by $\phi = \tan^{-1}H/2H_e$.

The external magnetic field also has the effect of tilting the axis of quantization of the nuclear spins with respect to the axis of quantization of the electronic spins on the same sublattice. The angle between the electronic and nuclear spin axes is approximately given by $\theta = \tan^{-1}H/H_{\rm hf}$, where the hyperfine field $H_{\rm hf} = AS/g_N\mu_N$. If the hyperfine field is much smaller than the exchange field, as in the case of F^{19} in MnF_2, the main effect of H will be to introduce a term in the hyperfine interaction proportional to $I^+S_z\sin\theta$, thereby inducing a first-order Raman relaxation process. If the canting angle ϕ is not too large, the sublattices may still be considered antiparallel, and the Raman-process calculation of Sec. II is still valid.

In other cases, an example being the NMR of Mn^{55} in MnF_2, the hyperfine field may be comparable with the exchange field. Any attempt to introduce a significant angle θ between the nuclear and electronic spin axes will then produce a sufficient canting of the electronic spins to affect the antiferromagnetic spin-wave modes. We might then expect the Raman-process nuclear spin-lattice relaxation rate calculated in Sec. II to be modified. Furthermore, a second-order two-magnon process is induced which is not present in the absence of canting. This process arises from three-magnon exchange-interaction terms of the form $2JS_xS_z\sin2\phi$, in a manner analogous to the exchange-scattering induced three-magnon process discussed in Sec. III. This two-magnon process is permitted because the application of a canting field normal to the z direction breaks down the symmetry which requires the conservation of the z component of total angular momentum.

B. Spin Waves in Canted Antiferromagnets

The first step in the calculation of the relaxation rate due to these two processes is to determine the spin-wave modes of a two sublattice canted antiferromagnet.[14] We write the Hamiltonian

$$\mathcal{H} = \sum_{j,i}\{2J\mathbf{S}_{i'}\cdot\mathbf{S}_{j'} - g\beta H(S_{ix'}+S_{jx'}) - g\beta H_{A1}(S_{iz'}-S_{jz'}) + (g\beta H_{A2}/2S)(S_{iy'}{}^2+S_{jy'}{}^2)\}, \tag{4.1}$$

where the primed coordinate system (x', y', z') is defined by the crystal axes. The easy-axis anisotropy field H_{A1} establishes the z' direction as a preferred axis of the spin alignment. The hard-axis anisotropy field H_{A2} makes the x'-z' plane an easy plane of magnetization. Generally only one type of anisotropy dominates. H_{A2} is set equal to zero in the case of easy-axis antiferromagnets such as MnF_2, and H_{A1} may often be neglected in the case of hard-axis canted antiferromagnets such as $CsMnF_3$. The static magnetic field H, applied in the x' direction, cants the spins away from z' axis by an angle $\phi = \tan^{-1}H/(2H_e+H_{A1})$. Here J is the magnitude of the exchange interaction between nearest-neighboring spins. The subscripts i and j refer to the two sublattices of N spins each. The equilibrium orientation of the spins is shown in Fig. 10.

We now define two unprimed coordinate systems, (x_i, y_i, z_i) and (x_j, y_j, z_j), by taking the z_i direction to be the equilibrium direction of the spins on the i sublattice and z_j to be the equilibrium direction of the j sublattice spins. The transformation from the primed coordinate system to the i system and the j system is accomplished by clockwise rotations in the x'-z' plane of ϕ and π-ϕ, respectively.

Using the new coordinate systems, we define the spin components for the two sublattices in terms of the magnon creation and annihilation operators $c_{\rm k}{}^\dagger$, $c_{\rm k}$, $d_{\rm k}{}^\dagger$, and $d_{\rm k}$, which obey the usual boson commutation relations. Then,

$$S_{ix}+iS_{iy} = S_i{}^+ = (2S/N)^{1/2}\{\sum_k \exp(-i\mathbf{k}\cdot\mathbf{r}_i)c_k + \cdots\},$$

$$S_{ix}-iS_{iy} = S_i{}^- = (2S/N)^{1/2}\{\sum_k \exp(i\mathbf{k}\cdot\mathbf{r}_i)c_k{}^\dagger + \cdots\},$$

$$S_{iz} = S - N^{-1}\sum_{k,k'}\exp[i(\mathbf{k}-\mathbf{k}')\cdot\mathbf{r}_i]c_k{}^\dagger c_{k'}, \tag{4.2}$$

and

$$S_{jx}+iS_{jy} = S_j{}^+ = (2S/N)^{1/2}\{\sum_k \exp(-i\mathbf{k}\cdot\mathbf{r}_j)d_k + \cdots\},$$

$$S_{jx}-iS_{jy} = S_j{}^- = (2S/N)^{1/2}\{\sum_k \exp(i\mathbf{k}\cdot\mathbf{r}_j)d_k{}^\dagger + \cdots\},$$

$$S_{jz} = S - N^{-1}\sum_{k,k'}\exp[i(\mathbf{k}-\mathbf{k}')\cdot\mathbf{r}_j]d_k{}^\dagger d_{k'}. \tag{4.3}$$

Transforming (4.1) to the new coordinate systems, and using (4.2) and (4.3), we obtain

$$\begin{aligned}\mathcal{H} = \sum_k\{&\tfrac{1}{2}A_k(c_k{}^\dagger c_k + d_k{}^\dagger d_k) + B_k c_k{}^\dagger d_k - C_k c_k d_{-k} - D_k(c_k c_{-k} + d_k d_{-k}) + \text{c.c.}\}\\ &- Jz(2s/N)^{1/2}\sin2\phi\sum_{k_1,k_2,k_3}\{\gamma_1(c_1 d_2{}^\dagger d_3 - d_1 c_2{}^\dagger c_3) + \text{c.c.}\}\delta(\mathbf{k}_1-\mathbf{k}_2+\mathbf{k}_3)\\ &+ (g\beta H/8S)(2S/N)^{1/2}\sum_{k_1,k_2,k_3}[(c_1{}^\dagger c_2 c_3 + \text{c.c.}) - (d_1{}^\dagger d_2 d_3 + \text{c.c.})]\delta(\mathbf{k}_1-\mathbf{k}_2-\mathbf{k}_3),\end{aligned} \tag{4.4}$$

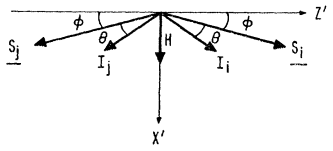

FIG. 10. The equilibrium spin configuration in a canted antiferromagnet. The canting is induced by a static magnetic field H applied along the x' axis.

where c.c. designates the complex conjugate of the other terms within the bracket, z is the number of nearest neighbors, and

$$\gamma_k = z^{-1}\sum_{\delta} \exp(i\mathbf{k}\cdot\boldsymbol{\delta}), \tag{4.5}$$

where $\boldsymbol{\delta}$ is the vector between nearest neighbors. To second order in ϕ,

$$\begin{aligned} A_k &= g\beta(H_e + H_{A1} + \tfrac{1}{2}H_{A2}),\\ B_k &= g\beta H_e \gamma_k \phi^2,\\ C_k &= g\beta H_e \gamma_k (1-\phi^2),\\ D_k &= \tfrac{1}{4}(g\beta H_{A2}). \end{aligned} \tag{4.6}$$

As in the case of the ordinary antiferromagnet, the exchange field is defined as $H_e = 2JzS/g\beta$. We drop the three-magnon term and diagonalize the Hamiltonian (4.4) by means of the transformation

$$\begin{aligned} c_k &= (s_k\alpha_k - t_k\alpha_{-k}^{\dagger}) + (u_k\beta_k + v_k\beta_{-k}^{\dagger}),\\ d_k &= (s_k\alpha_k - t_k\alpha_{-k}^{\dagger}) - (u_k\beta_k + v_k\beta_{-k}^{\dagger}). \end{aligned} \tag{4.7}$$

The new spin-wave operators α_k, $\alpha_k^{\dagger}$, β_k, and $\beta_k^{\dagger}$ obey boson commutation relations. The transformation coefficients are defined by the relations

$$\begin{aligned} s_k^2 + t_k^2 &= (A_k + B_k)/2\omega_{k\alpha},\\ -2s_k t_k &= (C_k + 2D_k)/2\omega_{k\alpha},\\ u_k^2 + v_k^2 &= (A_k - B_k)/2\omega_{k\beta},\\ -2u_k v_k &= (C_k - 2D_k)/2\omega_{k\beta}. \end{aligned} \tag{4.8}$$

In the long-wavelength limit, the normal mode frequencies are given by

$$\begin{aligned} \omega_{k\alpha}^2/\gamma^2 &= H_{AE1}^2 + H^2 + H_e^2 b^2 k^2 a^2,\\ \omega_{k\beta}^2/\gamma^2 &= H_{AE1}^2 + H_{AE2}^2 + H_e^2 b^2 k^2 a^2, \end{aligned} \tag{4.9}$$

where $H_{AE1}^2 = 2H_eH_{A1}$, $H_{AE2} = 2H_eH_{A2}$, $\gamma = g\beta/\hbar$, $b^2 = 2/z$, and a is the distance between nearest neighbors.

C. First-Order Raman Process

We now examine the first-order Raman nuclear spin-lattice relaxation process. Although the results to be derived here are valid when the hyperfine interaction is isotropic, we treat the more general case where the interaction is nonisotropic, but is diagonal along the axis of quantization of the electron spins. The hyperfine-interaction term responsible for the first-order Raman process is then $\mathcal{H}' = \frac{1}{2}A_zI^+S_z\sin\theta$. In Sec. II the transformation (2.4) was used in the calculation of the relaxation rate. Here we use the transformation (4.7), which takes into account the effect of the canting of the electron-spin sublattices on the spin-wave spectrum. With this transformation we obtain

$$\begin{aligned} \mathcal{H}' = -(A_zI^+/2N)\sin\theta \sum_{k_1,k_2}\{&(s_1s_2 + t_1t_2)\alpha_1^{\dagger}\alpha_2\\ &+ (u_1u_2 + v_1v_2)\beta_1^{\dagger}\beta_2 + (s_1u_2 - t_1v_2)(\alpha_1^{\dagger}\beta_2 + \alpha_1\beta_2^{\dagger})\}. \end{aligned} \tag{4.10}$$

From this we obtain the relaxation rate

$$\begin{aligned} T_1^{-1}(\text{Raman}) = (4\pi/\hbar)(A_z/2N)^2\sin^2\theta &\times \sum_{k_1,k_2}\{(s_1s_2 + t_1t_2)^2 n_{1\alpha}(1+n_{2\alpha})\\ &+ \delta_{1\alpha,2\alpha} + (u_1u_2 + v_1v_2)^2 n_{1\beta}(1+n_{2\beta})\delta_{1\beta,2\beta}\\ &+ 2(s_1u_2 - t_1v_2)^2 n_{1\alpha}(1+n_{2\beta})\delta_{1\alpha,2\beta}\}, \end{aligned} \tag{4.11}$$

where the subscripts on the δ functions refer to the magnon energies: e.g., $\delta_{1\alpha,2\beta}$ requires that $\hbar\omega_{\alpha}(k_1) = \hbar\omega_{\beta}(k_2)$. In the long-wavelength limit,

$$(s_1s_2 + t_1t_2)^2\delta_{1\alpha,2\alpha} \approx \omega_e^2\delta_{1\alpha,2\alpha}/4\omega_{1\alpha}^2, \tag{4.12a}$$

$$(u_1u_2 + v_1v_2)^2\delta_{1\beta,2\beta} \approx \omega_e^2\delta_{1\beta,2\beta}/4\omega_{1\beta}^2, \tag{4.12b}$$

$$(s_1u_2 - t_1v_2)^2\delta_{1\alpha,2\beta} \approx \delta_{1\alpha,2\beta}/4. \tag{4.12c}$$

The contribution of (4.12c) to the relaxation rate will be smaller than that of (4.12a) and (4.12b) by a factor of approximately $(k_BT/\hbar\omega_e)^2$, hence only the first two terms of (4.11) are retained. The sums in (4.11) are converted to integrals and are evaluated for the two cases: (1) $H_{A1} \gg H_{A2}$, and (2) $H_{A1} \ll H_{A2}$. For the first case, characteristic of easy-axis antiferromagnets such as MnF_2, we obtain

$$\begin{aligned} T_1^{-1}(\text{Raman}) = [4/(2\pi)^3 b^6](A_z^2/\hbar^2\omega_e)\sin^2\theta &\\ \times (k_BT/\hbar\omega_e)^3[I(x_0) + I(x_{AE1})], & \end{aligned} \tag{4.13}$$

where

$$\begin{aligned} x_0 &= T_0/T = g\beta(H^2 + H_{AE1}^2)^{1/2}/k_BT,\\ x_{AE1} &= T_{AE1}/T = g\beta H_{AE1}/k_BT, \end{aligned}$$

and the integral $I(x_0)$ is given by

$$I(x_0) = \int_{x_0}^{\infty} \frac{x\,dx}{e^x - 1}. \tag{4.14}$$

$I(x_{AE1})$ is defined similarly, with x_{AE1} as the lower limit. This is the same integral encountered in (2.20), the Raman-process nuclear spin-lattice relaxation rate in the absence of canting. When $H_0 \ll H_{AE1}$, as is often the case, x_0 is nearly equal to x_{AE1} and (4.14) reduces to the result (2.20). Thus, we see that the canting of the electronic spin sublattices has little effect upon the first-order Raman-process relaxation rate, other than a slight modification of the spin-wave energy gap.

The second case, in which $H_{A1}\ll H_{A2}$, describes an antiferromagnet with hard-axis anisotropy, such as $CsMnF_3$. In this limit we obtain

$$T_1^{-1}(\text{Raman})=[4/(2\pi)^3 b^6](A_z^2/\hbar^2\omega_e)\sin^2\theta \times(k_BT/\hbar\omega_e)^3[I(x_0)+I(x_{AE2})], \quad (4.15)$$

where $x_{AE2}=g\beta H_{AE2}/k_BT$. Usually, $x_{AE2}\gg x_0$. The integral is given by (4.14).

D. Second-Order Two-Magnon Process

The calculation of the second-order two-magnon relaxation rate proceeds in a fashion similar to the calculations of Sec. III. For small θ, the one-magnon term in the hyperfine interaction proportional to I^+ is

$$3\mathcal{C}^{(1)}=\tfrac{1}{2}A_\perp I^+(2S/N)^{1/2}\sum_{\mathbf{k}}(s_k\alpha_{\mathbf{k}}{}^\dagger-t_k\alpha_{\mathbf{k}}+u_k\beta_{\mathbf{k}}{}^\dagger+v_k\beta_{\mathbf{k}}), \quad (4.16)$$

where $A_\perp=\frac{1}{2}(A_x+A_y)$. This interaction may relax a nuclear spin while emitting or absorbing a virtual magnon. This virtual magnon may then be scattered by a thermal magnon via the three-magnon term in the electron Hamiltonian (4.4) which, after transformation to the normal-mode spin-wave operators is given by

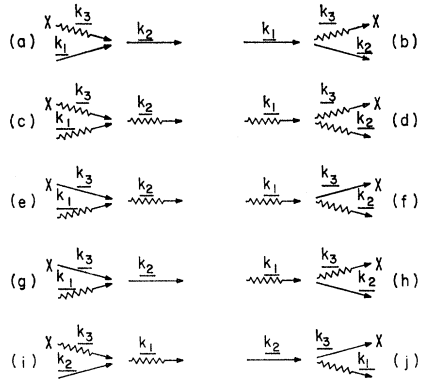

FIG. 11. The second-order dipolar scattering induced Raman process in antiferromagnets. These 10 diagrams result in four distinct two-magnon processes.

$$3\mathcal{C}^{(3)}=-2Jz(2S/N)^{1/2}\sin2\phi\sum_{\mathbf{k}_1,\mathbf{k}_2,\mathbf{k}_3}\{(2u_1s_2t_3+v_1t_2s_3)\beta_1\alpha_2{}^\dagger\alpha_3-(s_1u_2s_3+t_1v_2t_3)\alpha_1\beta_2{}^\dagger\beta_3 +[(u_1u_2u_3+v_1v_2v_3)+2(u_1v_2v_3+v_1u_2u_3)]\beta_1\beta_2{}^\dagger\beta_3+\text{c.c.}\}\delta(\mathbf{k}_1-\mathbf{k}_2+\mathbf{k}_3). \quad (4.17)$$

Here we have made the long-wavelength approximation of setting γ_k equal to unity. This scattering results in the second-order two-magnon processes diagrammed in Fig. 11. The matrix element for this process is

$$3\mathcal{C}^{(2)}=(2JzS/N)A_\perp I^+\sin2\phi\sum_{\mathbf{k}_1,\mathbf{k}_2,\mathbf{k}_3}\{M_1\alpha_1\alpha_2{}^\dagger+M_2\beta_1\beta_2{}^\dagger +M_3\beta_1\alpha_2{}^\dagger+M_4\beta_1{}^\dagger\alpha_2\delta(\mathbf{k}_1-\mathbf{k}_2+\mathbf{k}_3)\}. \quad (4.18)$$

The matrix elements M_i are determined by (4.16) and (4.17), and are given in the long-wavelength limit by

$$M_1{}^2\delta_{1\alpha,2\alpha}\approx\delta_{1\alpha,2\alpha}/64(\hbar\omega_{1\alpha})^2, \quad (4.19a)$$

$$M_2{}^2\delta_{1\beta,2\beta}\approx\delta_{1\beta,2\beta}/64(\hbar\omega_{1\beta})^2, \quad (4.19b)$$

$$(M_3{}^2+M_4{}^2)\delta_{1\beta,2\alpha}\approx\omega_e{}^2\delta_{1\beta,2\alpha}/\hbar^2\omega_{3\alpha}{}^4. \quad (4.19c)$$

From (4.18) we obtain the exchange-scattering-induced two-magnon spin-lattice relaxation rate

$$1/T_1{}^{(2)}=(4\pi/\hbar)(\hbar\omega_e/N)^2A_\perp{}^2\sin^2\!2\phi \times\sum_{\mathbf{k}_1,\mathbf{k}_2,\mathbf{k}_3}\{M_1{}^2n_{1\alpha}(1+n_{1\alpha})\delta_{1\alpha,2\alpha} +M_2{}^2n_{1\beta}(1+n_{2\beta})\delta_{1\beta,2\beta} +(M_3{}^2+M_4{}^2)n_{1\beta}(1+n_{2\alpha})\delta_{1\beta,2\alpha}\}\delta(\mathbf{k}_1-\mathbf{k}_2+\mathbf{k}_3). \quad (4.20)$$

Expression (4.19c), which arises from processes involving one spin wave of each mode, is by far the largest of the three expressions (4.19). We then evaluate (4.20) in the long-wavelength limit, replacing sums by integrals, and retaining only the terms proportional to (4.19c). We assume $H\ll H_e$, so that $\sin2\phi\approx H/H_e$. Again, we consider the two cases: (1) $H_{A1}\gg H_{A2}$, and (2) $H_{A1}\ll H_{A2}$. For the first case, that of an antiferromagnet with easy-axis anisotropy, we obtain

$$\frac{1}{T_1{}^{(2)}}=\frac{8}{(2\pi)^3b^6}\frac{A_\perp{}^2}{\hbar^2\omega_e}\left(\frac{k_BT}{\hbar\omega_e}\right)^3\frac{H_0{}^2}{H_0{}^2+H_{AE1}{}^2}I^{(2)}(x_0), \quad (4.21)$$

with

$$I^{(2)}(x_0)=\int_{x_0}^{\infty}\frac{2x^2(x^2-x_0{}^2)}{4x^2-3x_0{}^2}\frac{e^xdx}{(e^x-1)^2}. \quad (4.22)$$

Again, we define $x_0=g\beta(H^2+H_{AE1}{}^2)^{1/2}k_BT$. The integral $I^{(2)}(x_0)$ for the exchange-scattering-induced two-magnon process and the integral $I(x_0)$ (4.14) for the first-order Raman process are plotted as a function of x_0^{-1} in Fig. 12. For $x_0\ll1$, the two integrals have nearly the same temperatures dependence at temperature high compared with the spin-wave energy gap. In this temperature range,

$$T_1(\text{Raman})/T_1{}^{(2)}=(A_\perp H_{\text{hf}})^2/A_zH_{AE1})^2$$

for $H\ll H_{AE1}$ and $H\ll H_{\text{hf}}$. For parameters typical of F^{19} in MnF_2, this ratio is 0.22, indicating that the first-order Raman process is the more effective in relaxing the F^{19} nuclear spins. The hyperfine field at the nucleus of Mn^{55} in MnF_2 is much larger than the F^{19} transferred hyperfine field, however, and the ratio is 6.7 for Mn^{55}

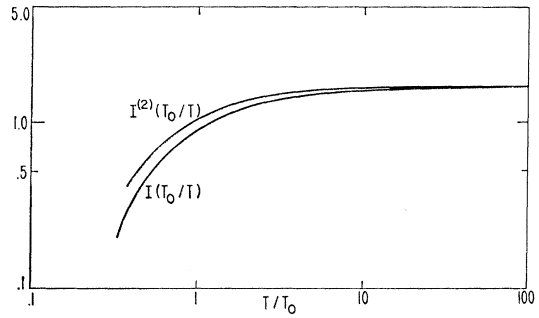

FIG. 12. The temperature-dependent integrals $I(T_0/T)$ and $I^{(2)}(T_0/T)$, which occur, respectively, in the first-order and in the second-order Raman-process relaxation-rate calculation for canted easy-axis antiferromagnets.

nuclear spin-lattice relaxation. Thus the second-order process should be of greater significance in the relaxation of Mn^{55}. Since the first-order process arises from the creation and annihilation of spin waves of the same mode, and the second-order process involves the creation of a spin wave from one mode and the annihilation of one from the other mode, the two processes do not interfere. Thus the total relaxation rate is equal to the sum of the relaxation rates from the first- and second-order two-magnon processes.

For an antiferromagnet with hard-axis isotropy, $H_{A1}\ll H_{A2}$. The evaluation of (4.20) in this limit gives the result

$$\frac{1}{T_1^{(2)}}=\frac{16}{(2\pi)^3 b^6}\frac{A^2}{\hbar^2\omega_e}\left(\frac{H}{H_{AE2}}\right)^2\left(\frac{k_BT}{\hbar\omega_e}\right)^3\frac{k_BT}{g\beta H_{AE2}}I(x_{AE2},x_0), \tag{4.23}$$

where

$$I^{(2)}(x_{AE2},x_0)=\int_{x_{AE2}}^{\infty}\frac{x^2[(x^2-x_{AE2}^2)(x^2-x_0^2)]^{1/2}}{1+4(x_{AE2}^2+x_0^2)(x^2-x_{AE2}^2)/x_{AE2}^4}\frac{e^x}{(e^x-1)^2}dx. \tag{4.24}$$

For typical values of H_{AE2} and $H_{\rm hf}$, (4.23) gives a relaxation rate one order of magnitude larger than that obtained from (4.15).

When $g\beta H_{AE2}/k_BT\ll 1$ and $(H_0^2+H_{AE1}^2)/H_{AE2}^2\ll 1$, (4.24) reaches its maximum value of 26.0. In Fig. 13 the integral is plotted as a function of

$$x_0=g\beta(H^2+H_{AE1}^2)^{1/2}/k_BT \quad \text{for} \quad x_{AE2}=2.2.$$

This corresponds to the hard-axis anisotropy field of $CsMnF_3$ with $T=4.2°K$. In Fig. 14, $I^{(2)}(x_{AE2},x_0)$ is plotted as a function of x_{AE2}^{-1} for $x_0/x_{AE2}=0.083$, which corresponds to a canting field of 5800 Oe applied to $CsMnF_3$. When Figs. 13 and 14 are used to examine the field and temperature dependence of (4.23), the results obtained are in qualitative agreement with the experimental results obtained by Welsh,[3] who found the nuclear spin-lattice relaxation rate of Mn^{55} in $CsMnF_3$ to be proportional to T^5 and approximately proportional to the 1.3 power of the applied field. The temperature dependence calculated from (4.23) varies from T to the fifth power at high temperatures to slightly over the sixth power at lower temperatures. The field dependence calculated here is approximately $H^{1.9}$, and at low fields the relaxation rates obtained are nearly one order of magnitude slower than those measured by Welsh. The incomplete agreement with experiment suggests the existence of another important relaxation process with a lower field dependence.

E. Three-Magnon Relaxation Process

The relaxation rate due to the first-order three-magnon process has been calculated by Welsh[3] and was found to be three orders of magnitude smaller than the observed rates. However, the antiferromagnetic exchange-scattering-enhanced relaxation rate calculated in Sec. III becomes infinite for a vanishing energy gap in the spin-wave spectrum. This suggests that second-order three-magnon processes involving spin waves from the α branch only may give a significant contribution to the relaxation rate. Any processes involving either virtual or thermal magnons from the β branch will have energy denominators containing the much larger energy gap $g\beta H_{AE2}$, and may be neglected. Thus the hyperfine interaction term of interest is

$$\mathcal{H}^{(1)}=\tfrac{1}{2}A_\perp(2S/N)^{1/2}I^+\sum_k s_k(\alpha_k^\dagger+\alpha_k), \tag{4.25}$$

where we make the approximation $s_k\approx -t_k\approx(\omega_e/4\omega_k)^{1/2}$. The virtual magnon emitted of absorbed while relaxing the nuclear spin via (4.25) is scattered by thermal magnon via the four-magnon exchange interaction. When the transformation (4.7) is applied, and terms containing β mode magnons are discarded, the exchange interaction becomes

$$\begin{aligned}\mathcal{H}^{(4)}=&-(Jz/2N)b^2a^2\\&\times\sum_{k_1,k_2,k_3,k_4}\{\alpha_1^\dagger\alpha_2^\dagger\alpha_3\alpha_4+4\alpha_1\alpha_2\alpha_3^\dagger\alpha_{-4}\\&+4\alpha_1^\dagger\alpha_{-2}\alpha_3\alpha_{-4}^\dagger+\text{c.c.}\}s_1s_2s_3s_4\\&\times(\mathbf{k}_1\cdot\mathbf{k}_2+\mathbf{k}_3\cdot\mathbf{k}_4)\delta(\mathbf{k}_1+\mathbf{k}_2-\mathbf{k}_3-\mathbf{k}_4).\end{aligned} \tag{4.26}$$

The matrix element for the second-order three-magnon process is then

$$\begin{aligned}\mathcal{H}^{(3)}=&-(AI^+/4NS)(2S/N)^{1/2}\\&\sum_{k_1,k_2,k_3,k_4}s_1s_2s_3[M](\alpha_1^\dagger\alpha_2^\dagger\alpha_3+\alpha_1\alpha_2\alpha_3^\dagger)\\&\times\delta(\mathbf{k}_1+\mathbf{k}_2-\mathbf{k}_3-\mathbf{k}_4),\end{aligned} \tag{4.27}$$

where

$$M=\frac{2(\mathbf{k}_1\cdot\mathbf{k}_3+\mathbf{k}_2\cdot\mathbf{k}_4)-(\mathbf{k}_1\cdot\mathbf{k}_2+\mathbf{k}_3\cdot\mathbf{k}_4)}{k_0^2+k_4^2}, \tag{4.28}$$

with $k_0=g\beta(H^2+H_{AE1}^2)^{1/2}/\hbar\omega_e ab$. From (4.27) we ob-

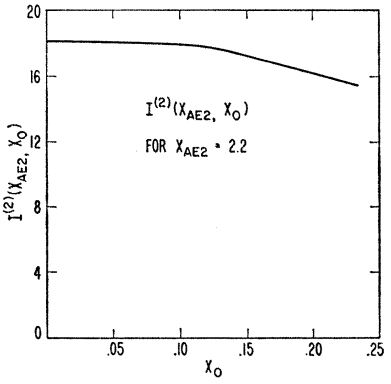

FIG. 13. The temperature-dependent integral $I^{(2)}(x_{AE2}, x_0)$ which occurs in the calculation of the relaxation rate due to the second-order Raman process in canted hard-axis antiferromagnets. The integral is plotted as a function of x_0, for $x_{AE2}=2.2$.

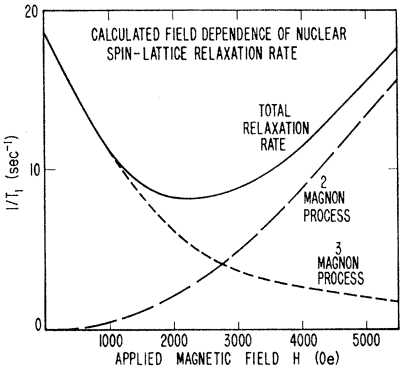

FIG. 15. The field dependence of the calculated nuclear spin-lattice relaxation rate of Mn^{55} in $CsMnF_3$. $1/T_1$ is plotted as a function of H for the second-order two-magnon and three-magnon processes. The sum of these two relaxation rates is also displayed.

tain the second-order three-magnon relaxation rate

$$1/T_1^{(3)}=(4\pi/\hbar)(A_\perp^2/4N^3S)\times\sum_{k_1,k_2,k_3}(s_1s_2s_3)(M)^2n_1n_2(1+n_3)\delta(E_1+E_2-E_3). \tag{4.29}$$

Replacing the sums by integrals, we evaluate (4.29) in the long-wavelength limit, taking $x_0\ll 1$. We then find

$$1/T_1^{(3)}=[A_\perp^2/32Sb^9(2\pi)^4\hbar^2\omega_e](k_BT/\hbar\omega_e)^5I^{(3)}(x_0), \tag{4.30}$$

where

$$I^{(3)}(x_0)=\int_{x_0}^{\infty}\int_{x_0}^{\infty}\frac{dx_1dx_2}{2x_0}\frac{[x_1^2+x_2^2+x_1^2x_2^2]e^{x_1+x_2}}{(e^{x_1}-1)(e^{x_2}-1)(e^{x_1+x_2}-1)}. \tag{4.31}$$

For $x_0\ll 1$, the integral may be approximated by

$$1^{(3)}(x_0)\approx(24.7/x_0)[\ln 1/x_0+1.22]. \tag{4.32}$$

Equations (4.30) and (4.32) are used to calculate the exchange-scattering-induced three-magnon-process nuclear spin-lattice relaxation rate of Mn^{55} in $CsMnF_3$ at 4.2°K. The result is plotted as a function of applied field in Fig. 15. The exchange-scattering-induced two-magnon-process relaxation rate $1/T_1^{(2)}$ calculated from (4.23) is also plotted, as is the total relaxation rate $1/T_1^{(2)}+1/T_1^{(3)}$. The total relaxation rate increases as $H^{1.46}$ at high fields, but has a point of inflection around 2000 Oe. This increase in relaxation rate at low fields was not observed by Welsh,[22] whose measurements extended to fields as low as 600 Oe. The three-magnon process relaxation rate calculated here for $CsMnF_3$ is not accurate at low fields, however. If we consider the effect of H_N, the field due to the hyperfine interaction with the nuclear spin, the energy gap in the spin-wave spectrum with zero applied field is $g\beta[2h_e(H_{A1}+H_N)]^{1/2}$, where H_N is inversely proportional to the nuclear spin

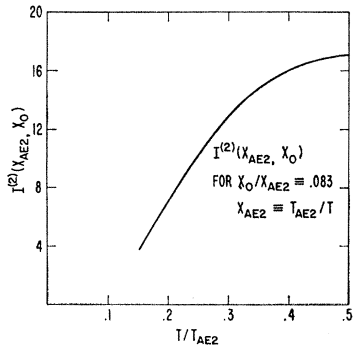

FIG. 14. The integral $I^{(2)}(x_{AE2},x_0)$ plotted as a function of $(x_{AE2})-1$, for $x_0/x_{AE2}=0.083$. Here $x_{AE2}\equiv T_{AE2}/T$ and $x_0\equiv T_0/T$.

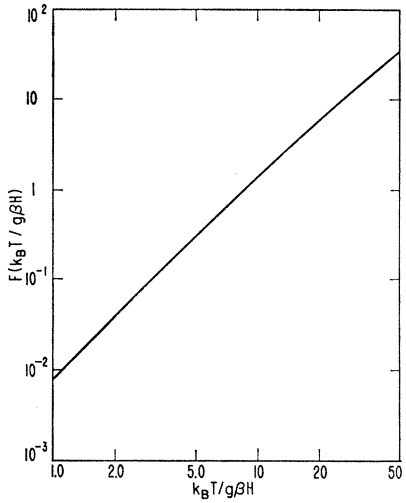

FIG. 16. Plot of the function $F(k_BT/g\beta H)$, which occurs in the ferromagnetic dipolar induced two-magnon process.

[22] K. Lee, A. M. Portis, and G. L. Witt, Phys. Rev. **132**, 144 (1963).

temperature. Often, H_N may be neglected in comparison with H_{A1}. However, the "easy axis" anisotropy of $CsMnF_3$ is quite small, being only 1.1 Oe, whereas $H_N=2.2$ Oe when the nuclear spin temperature is equal to the lattice temperature of 4.2°K. At this spin temperature, the zero-field relaxation rate is only one-half the rate for infinite nuclear spin temperature. Thus, for finite nuclear spin temperature, the point of inflection of the total relaxation rate curve is shifted to a lower field than that of the curve shown in Fig. 16.

Over most of the range of temperatures and fields investigated by Welsh, the experimental value of $1/T_1$ is larger than the total rate calculated from Eqs. (4.24) and (4.30) by a factor of 4. Possibly, this discrepancy may be explained by the fact that $CsMnF_3$ is a much more complicated system than the simple two-sublattice model discussed here. The $CsMnF_3$ unit cell consists of six ferromagnetic planes stacked antiferromagnetically along the c axis.[22] The calculations given here consider only the nearest-neighbor exchange interaction, which is antiferromagnetic. Welsh has shown that the next-nearest-neighbor ferromagnetic exchange interaction significantly affects the spin-wave spectrum. Welsh has also shown that the spin-wave spectrum in $CsMnF_3$ is anisotropic, whereas the spin-wave density of states used in our calculations is based upon a spherical-band model. Furthermore, we have no assurance that the long-wave-length approximation used here is appropriate, since the true density of states at the band edges is not known.

Mahler, Daniel, and Parrish[23] have recently measured the zero field T_1's of the F^{19} nuclei in the canted system $KMnF_3$, finding a low-temperature exponential regime and power laws (T^5 or T^7 for different samples) at higher temperatures. As indicated in this section, the T^5 behavior is somewhat characteristic of canted structures and may indeed be an intrinsic process as suggested by the authors. However, we have not carried out a detailed calculation for this four-sublattice system because of some uncertainties with regard to the detailed nature of the hyperfine interaction at the two fluorine sites. Such studies are feasible and would very likely lead to interesting results.

V. DIPOLAR INDUCED TWO-MAGNON PROCESS

A. Ferromagnetic Case

In Sec. IV we saw that although a slight canting of the antiferromagnetic sublattices produces a comparatively small perturbation in the spin-wave spectrum, it may have a significant effect upon the nuclear spin-lattice relaxation rate by breaking the symmetry of the system, thus inducing a two-magnon process which would otherwise be forbidden. In this section we shall see that the electron magnetic dipole-dipole interaction creates a similar situation in ferromagnets and noncanted antiferromagnets.

In the presence of the dipole-dipole interaction, the long-wavelength spin-wave dispersion relation for cubic ferromagnets[24] becomes

$$\hbar\omega_k=g\beta[(H_0+H_ek^2a^2)(H_0+4\pi M\sin^2\theta_k+H_ek^2a^2)]^{1/2}. \tag{5.1}$$

Here H_0 is the applied magnetic field corrected for static demagnetization effects, M is the saturation magnetization of the ferromagnet, and θ_k is the angle between the z axis and the direction of propagation of the spin wave. If $M\ll H_0$, (5.1) reduces to (2.16), the dispersion relation in the absence of the dipolar interaction. Since the applied field must be much larger than the magnetization to ensure single domain behavior of the ferromagnet, we may almost always use (2.16) in place of (5.1). Thus, the dipole-dipole interaction should have little effect upon the relaxation processes calculated in the preceding sections. The importance of this interaction lies in the fact that it does not commute with the z component of total electron-spin angular momentum. Therefore this quantity need not be conserved, and a two-magnon relaxation process is allowed. The second-order process occurs in the following manner:[25]

(1) A nuclear spin flips and creates a virtual spin

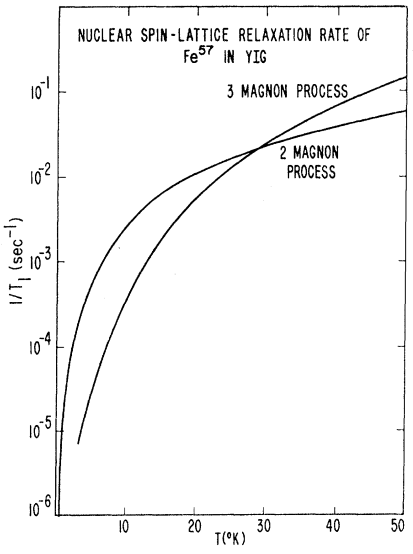

FIG. 17. The calculated nuclear spin-lattice relaxation rate of Fe^{57} in YIG for the dipolar induced two-magnon process and the exchange-scattering-enhanced three-magnon process, with $H=5\times10^3$Oe.

[23] R. J. Mahler, A. C. Daniel, and P. T. Parrish, Phys. Rev. Letters **19**, 85 (1967).

[24] See, e.g., C. Kittel, *Quantum Theory of Solids* (John Wiley & Sons, Inc., New York, 1963), Chap. 4.

[25] D. Beeman, J. Appl. Phys. **38**, 1276 (1967).

wave, via the transverse part of the hyperfine interaction $\frac{1}{2}AI^+S^-$.

(2) This virtual magnon is then scattered by a thermal magnon, via the part of the electronic dipole-dipole interaction proportional to S_zS^+. This three-magnon term is given by[26]

$$H_d^{(3)}=-2\pi g\beta(2g\beta M/V)^{1/2}\times\sum_{\mathbf{k},\mathbf{k}',\mathbf{k}''}(k^-k^z/k^2)b_kb_{k'}{}^\dagger b_{k''}\delta(\mathbf{k}-\mathbf{k}'+\mathbf{k}''),\quad(5.2)$$

where M is the saturation magnetization of the ferromagnet, $b_k{}^\dagger$ and b_k represent, respectively, magnon creation and annihilation operators, and $k^-=k_x-ik_y$. The effective matrix element for the second-order two-magnon process is then given by

$$H_{\text{eff}}^{(2)}=2\pi AI^+(g\beta M/N)\times\sum_{\mathbf{k},\mathbf{k}'}\left\{\frac{k^-k^z}{k^2}+\frac{(\mathbf{k}-\mathbf{k}')^-(\mathbf{k}-\mathbf{k}')^z}{(\mathbf{k}-\mathbf{k}')^2}\right\}\frac{b_k{}^\dagger b_{k'}}{E(\mathbf{k}-\mathbf{k}')}.\quad(5.3)$$

For a cubic lattice with the applied field $H\gg M$, $E(\mathbf{k}-\mathbf{k}')=g\beta H+\hbar\omega_e a^2(\mathbf{k}-\mathbf{k}')^2$.

Using this matrix element Fermi's golden-rule calculation of the spin-lattice relaxation rate gives

$$\frac{1}{T_1}=\frac{A^2}{\hbar^2\omega_e}\left(\frac{g\beta M}{\hbar\omega_e}\right)^2F\left(\frac{k_BT}{g\beta H}\right),\quad(5.4)$$

with

$$F\left(\frac{k_BT}{g\beta H}\right)=\frac{1}{10\pi}\left\{\frac{I_1}{3}\frac{k_BT}{g\beta H}+\frac{I_2}{4}\right\},\quad(5.5)$$

where

$$I_1=\int_{x_0}^{\infty}\frac{4x-7x_0}{4x-3x_0}\frac{e^x}{(e^x-1)^2}\,dx\quad(5.6)$$

and

$$I_2=\int_{x_0}^{\infty}\frac{dx}{x-x_0}\log\left(\frac{4x-3x_0}{x_0}\right)\frac{e^x}{(e^x-1)^2},\quad(5.7)$$

with $x_0=g\beta H/k_BT$. Here I_1 and I_2 were integrated numerically in order to calculate the function

$$F(k_BT/g\beta H),$$

which is plotted in Fig. 16. It may be seen from Fig. 16 that $F(k_BT/g\beta H)$ is nearly proportional to $(T/H)^2$ for $k_BT\gg g\beta H$. Using parameters typical of Fe^{57} in YIG, with $H=5\times10^3$ Oe, the two-magnon process gives $T_1^{-1}=10^{-3}F(T/0.7)$. The exchange-scattering-enhanced three-magnon process gives $T_1^{-1}=1.5(T/100)^{7/2}$. T_1^{-1} is plotted for the two processes in Fig. 17. The two-magnon process is faster up to about 30°K, where $T_1=50$ sec. Above this temperature, the three-magnon process dominates. For smaller values of H, the cross-over point will occur at higher temperatures, since the three-magnon process relaxation rate is relatively independent of H.

[26] M. Sparks, R. Loudon, and C. Kittel, Phys. Rev. **122**, 791 (1961).

B. Antiferromagnetic Case

The inclusion of dipolar terms in the calculation of the spin-wave spectrum of an antiferromagnet with easy-axis anisotropy results in corrections of order M/H_e.[27] Since M, the sublattice magnetization, is always much smaller than the exchange field, the only effect of the dipolar interaction on the nuclear spin-lattice relaxation is the introduction of a second-order two-magnon relaxation process similar to that discussed above for ferromagnets.

The hyperfine interaction term

$$\mathcal{H}^{(1)}=\tfrac{1}{2}AI^+(2S/N)^{1/2}\sum_k(u_k\alpha_k{}^\dagger+v_k\beta_k)\quad(5.8)$$

relaxes the nuclear spin and emits or absorbs a virtual magnon. The virtual magnon is scattered by a thermal magnon via the three-magnon terms of the dipole-dipole interaction

$$\mathcal{H}^{(3)}=-2\pi g\beta M(2/NS)^{1/2}\times\sum_{\mathbf{k}_1,\mathbf{k}_2,\mathbf{k}_3}\{(k_1^-k_{1z}/k_1^2)(c_1+d_1{}^\dagger)(c_2{}^\dagger c_3-d_2d_3{}^\dagger)+\text{c.c.}\}\times\delta(\mathbf{k}_1-\mathbf{k}_2+\mathbf{k}_3),\quad(5.9)$$

where the c and d magnon operators are expressed in terms of the α and β normal-mode magnon operators by the transformation (2.4). The result of this scattering is the second-order two-magnon interaction

$$\mathcal{H}^{(2)}=(2\pi g\beta MAI^+/N)\times\sum_{\mathbf{k}_1,\mathbf{k}_2,\mathbf{k}_3}\{M_1\alpha_2{}^\dagger\alpha_1+M_2\beta_2\beta_1{}^\dagger+M_3\alpha_2{}^\dagger\beta_1\},\quad(5.10)$$

where

$$M_1=\{(k_1^-k_{1z}/k_1^2)(u_1+v_1)[(u_3^2+v_3^2)u_2-(2u_3v_3)v_2]+(k_3^-k_{3z}/k_3^2)(u_3+v_3)^2(u_1u_2-v_1v_2)\}\times\delta(\mathbf{k}_1-\mathbf{k}_2+\mathbf{k}_3)/E_3,\quad(5.11a)$$

$$M_2=\{(k_3^-k_{3z}/k_1^2)(u_1+v_1)[(u_3^2+v_3^2)v_2-(2u_3v_3)u_2]-(k_3^-k_{3z}/k_3^2)(u_3+v_3)^2(u_1u_2-v_1v_2)\}\times\delta(\mathbf{k}_1-\mathbf{k}_2+\mathbf{k}_3)/E_3,\quad(5.11b)$$

$$M_3=\{(k_1^+k_{1z}/k_1^2)(u_1+v_2)[(u_3^2+v_3^2)u_2-(2u_3v_3)v_2]+(k_2^+k_{2z}/k_2^2)(u_2+v_2)[(u_3^2+v_3^2)v_1-(2u_3v_3)u_1]\}\times\delta(\mathbf{k}_1+\mathbf{k}_2-\mathbf{k}_3)/E_3,\quad(5.11c)$$

with $E_k=g\beta H(2H_eH_A+H_e{}^2k^2a^2b^2)^{1/2}$. Equation (5.10) is

[27] R. Loudon and P. Pincus, Phys. Rev. **132**, 673 (1963).

used to calculate the relaxation rate

$$T_1^{-1}=2(2\pi)^3(g\beta M)^2(A^2/\hbar N^2)\times\sum_{\mathbf{k}_1,\mathbf{k}_2,\mathbf{k}_3}\{|M_1|^2+|M_2|^2+|M_3|^2\}\times n_1(1+n_1)\delta(E_1-E_2). \quad (5.12)$$

Then (5.12) is evaluated in the long-wavelength limit, replacing the sums by integrals in the usual manner. The angular integrations are simplified if the direction of $\mathbf{k}_1$ is defined relative to the z direction and the direction of $\mathbf{k}_2$ is defined relative to $\mathbf{k}_1$. After all integrations are performed, we obtain the result

$$T_1^{-1}=\frac{2}{5\pi b^6}\frac{A^2}{\hbar^2\omega_e}\left(\frac{M}{H_{AE}}\right)^2\left(\frac{k_BT}{\hbar\omega_e}\right)^2 I_{\rm dip}\left(\frac{T_{AE}}{T}\right), \quad (5.13)$$

with $H_{AE}=(2H_eH_A)^{1/2}$. The integral $I_{\rm dip}$ is defined as

$$I_{\rm dip}\left(\frac{T_{AE}}{T}\right)=\int_{x_{AE}}^{\infty}\frac{x^4(2x^2-x_{AE}^2)}{x^2-x_{AE}^2}\left\{\frac{2(2x^2-x_{AE}^2)}{4x^2-3x_{AE}^2}-\frac{x_{AE}^2}{2(x^2-x_{AE}^2)}\ln\left(\frac{4x^2-3x_{AE}^2}{x_{AE}^2}\right)\right\}\frac{e^x dx}{(e^x-1)^2}, \quad (5.14)$$

where $x_{AE}=g\beta H_{AE}/k_BT=T_{AE}/T$. This integral, which is plotted as a function of x_{AE}^{-1} in Fig. 18, reaches a maximum value of 52.0 as x_{AE} approaches zero. The contribution of this process to the nuclear spin-lattice relaxation rate of MnF_2 has been calculated and is plotted as a function of temperature in Fig. 8. The relaxation rates due to the exchange-scattering-enhanced three-magnon process and the short-wavelength Raman process are also plotted. The latter process, which is discussed in the Appendix, gives by far the largest contribution to the relaxation rate. However, this process only occurs in materials having a crystal structure similar to MnF_2 and is not operative in an ideal two-sublattice antiferromagnet. Thus, in many cases the most significant contribution to the relaxation rate will be that from the exchange-scattering-enhanced three-magnon process and the dipolar induced two-magnon process. From Fig. 8, we see that the three-magnon process dominates at high temperatures, but that the two-magnon process is most important at low temperatures, where the three-magnon rate falls off exponentially as $\exp(-g\beta H_{AE}/k_BT)$.

We have neglected here the contribution to the relaxation rate from third and higher-order processes due to repeated scatterings of spin waves from the three-magnon dipolar term (5.9). Each scattering will contribute a factor of order $(M/H_{AE})^2$. Since this ratio is always small for the magnetizations and anisotropy field found in easy-axis antiferromagnets, the neglect of these higher-order terms is justified.

In Sec. IV, we saw that the energy gap of the α branch of the spin-wave spectrum may be quite small for hard-axis canted antiferromagnets. Thus the matrix element for the exchange-scattering-induced three-magnon process which involves only α-branch magnons will have the energy $E_{k\alpha}$ in the denominator, thus giving a much larger contribution to the relaxation rate than processes involving β-branch magnons. However, the three-magnon dipolar terms for a hard-axis antiferromagnet are like the three-magnon exchange terms, in that there is no scattering process involving only α-branch magnons. Thus the small energy denominators associated with the α branch will not occur. Therefore, when the canting field H is small, the three-magnon process relaxation rate will be much larger than that due to the dipolar-induced two-magnon process. The matrix element for the two-magnon exchange-scattering-induced process is larger than the matrix element for the dipolar-induced process by a factor of

$$MH_{AE2}/HH_e.$$

Since this ratio is much greater than unity unless H is very small, we may conclude that the dipolar-induced two-magnon process is never significant for hard-axis antiferromagnets.

VI. CONCLUSIONS

We have considered some second-order processes of nuclear spin-lattice relaxation which may enhance or supplant existing first-order processes. We have shown that in almost all cases, the relaxation rate will be significantly affected by these processes.

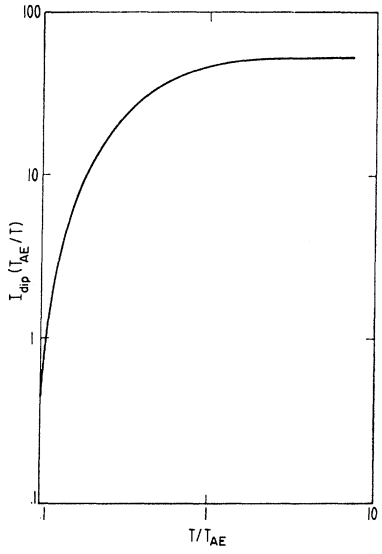

FIG. 18. The temperature-dependent integral $I_{\rm dip}(T_{AE}/T)$, which occurs in the calculation of the antiferromagnetic dipolar-induced two-magnon relaxation rate.

We have shown that the three-magnon relaxation process in both ferromagnets and antiferromagnets is significantly enhanced by the second-order three-magnon process. This process arises when a nuclear spin flips, creating a virtual spin wave which is scattered by a thermal magnon, via the exchange interaction. This will enhance the ferromagnetic three-magnon process relaxation rate by a factor of 8.[7] For antiferromagnets, the minimum enhancement is by a factor of 2.05, for $T \ll T_{AE}$, and the maximum enhancement increases as $(T/T_{AE})\ \ln T/T_{AE}$. Here T_{AE} is the temperature corresponding to the energy gap in the spin-wave spectrum. For temperatures on the order of T_{AE} the enhancement amounts to one order of magnitude.

In cases where the symmetry of the system dictates the conservation of the longitudinal component of a spin angular momentum, thus prohibiting the first-order two-magnon relaxation process, the electron magnetic dipole-dipole interaction destroys this symmetry, inducing a second-order Raman process. In the ferromagnetic case, the contribution to the relaxation rate from this process is approximately proportional to $(T/H)^2$. Since the three-magnon process rate is proportional to T^3, the second-order two-magnon process will dominate at low temperatures and at small applied fields H. In the antiferromagnetic case, this process yields a relaxation rate with a temperature dependence somewhat lower than the exchange-scattering-enhanced three-magnon process. Therefore the dipolar induced two-magnon process will dominate at very low temperatures.

The first-order Raman process is allowed in antiferromagnets when the axis of nuclear spin quantization is canted away from the axis of electronic spin quantization by an external magnetic field. This field also cants the electron-spin sublattices relative to each other, introducing three-magnon terms in the exchange interaction. We have shown that this leads to a second-order two-magnon process which may often be competitive with the first-order process. In easy-axis antiferromagnets, the anisotropy field H_A establishes a preferred axis of spin alignment. In this case the second-order-process relaxation rate has approximately the same temperature and field dependence as the first-order process and is faster by a factor of approximately $H_{\rm hf}^2/2H_eH_A$. Here $H_{\rm hf}$ is the hyperfine field at the nucleus, and H_e is the electronic exchange field. For the relaxation of nuclear spins in magnetic ions, this may represent a substantial increase in the relaxation rate over that due to the first-order process. When the hyperfine interaction is weak, as in the case of nonmagnetic ions having a transferred hyperfine interaction, the first-order process will usually dominate. In hard-axis antiferromagnets, in which there is a preferred plane of magnetization, the second-order Raman process relaxation rate is almost always considerably faster than the first-order process relaxation rate. Since hard-axis antiferromagnets usually have very weak in-plane anisotropy fields, the energy gap of one branch of the spin-wave spectrum is nearly proportional to the applied field H. When H is small, the exchange-scattering-enhanced three-magnon process can also give a significant contribution to the relaxation rate. In this context our calculations appear to be consistent with Welsh's measurements in $CsMnF_3$.

We have also discussed the possibility of further enhancement of the three-magnon relaxation process by repeated exchange scatterings of spin waves. Although no calculations have been performed for these higher-order processes, we believe that they may be of significance when the electronic spin S is not large. They may be particularly important in antiferromagnets when the energy gap in the spin-wave spectrum is much smaller than k_BT, and are therefore worthy of further study.

It should be emphasized that the relaxation rates plotted in Figs. 8, 15, and 17 were calculated using the long-wavelength approximation and are intended only to delineate and show the relative magnitudes of the various relaxation processes. In order to obtain accurate results which may be compared with experimentally obtained values of the relaxation rate, it is necessary to carry out the summations using the true spin-wave density of states for the particular material investigated.

ACKNOWLEDGMENTS

We would like to thank Professor V. Jaccarino, Dr. N. Kaplan, and Professor R. Loudon for their valuable contributions to the study of the relaxation of F^{19} in MnF_2. We have also benefited from discussions with Professor T. Holstein, Dr. L. B. Welsh, Dr. A. Narath, Dr. L. R. Walker, Professor R. Orbach, and Professor H. Meyer.